

TABLE 3  
SOURCES FROM 1LC 20 CM SURVEY

Name (1)	RA (2)	Dec (3)	1658 MHz			1281 MHz			$\alpha$ (10)	$\Theta$ (11)	Notes (12)
			$I$ (4)	$S$ (5)	$\theta$ (6)	$I$ (7)	$S$ (8)	$\theta$ (9)			
357.641−0.080 e	17 40 12.132	−30 59 04.81	...	...	...	89.7	1279.3	118.9	...	30.7	
357.666−0.107 e	17 40 22.284	−30 58 39.62	...	...	...	52.7	2783.9	60.7	...	29.1	GPSR, Gal
357.695−0.084 e	17 40 21.055	−30 56 27.60	...	...	...	52.9	1557.9	45.1	...	27.3	GPSR, Gal
357.768−0.985	17 44 06.581	−31 21 12.52	7.9	8.0	0.0	9.4	10.7	3.3	1.1	6.3	
357.795−0.789	17 43 23.853	−31 13 42.71	21.0	46.3	6.4	33.1	98.1	25.7	2.9	15.2	GPSR
357.806−1.047	17 44 26.965	−31 21 14.77	8.0	9.0	0.0	7.7	6.3	0.0	−1.4	4.7	GPSR
357.808−0.299	17 41 29.028	−30 57 31.43	36.2	20.7	0.0	53.4	124.9	9.7	7.0	24.7	GPSR
357.812−1.107	17 44 42.525	−31 22 48.60	17.7	19.9	2.2	14.1	16.1	2.6	−0.8	7.8	
357.840−0.881 m	17 43 52.350	−31 14 16.93	18.8	31.0	0.5	25.2	47.8	1.1	...	8.1	
357.842−0.877 m	17 43 51.815	−31 14 03.13	14.1	29.8	0.4	21.1	48.1	0.7	1.8	8.3	GPSR
357.862−0.997 m	17 44 23.257	−31 16 48.89	21.9	55.2	7.7	31.3	90.1	7.7	...	0.2	
357.865−0.996 m	17 44 23.595	−31 16 35.73	199.7	191.5	0.0	180.0	263.3	0.6	−0.5	0.0	GPSR, 1LC, VLA, xgal
357.866−0.995 m	17 44 23.553	−31 16 31.96	22.8	153.9	19.5	...	...	...	...	0.1	
357.885+0.005	17 40 28.258	−30 43 57.77	69.8	80.7	3.4	80.0	88.1	0.0	0.3	16.4	GPSR
357.901−1.052	17 44 42.358	−31 16 33.31	6.1	5.6	0.0	...	...	...	...	4.7	
357.906+0.108	17 40 06.963	−30 39 34.94	25.8	29.0	2.1	28.4	75.4	8.0	3.7	18.7	GPSR
357.945−0.134	17 41 10.188	−30 45 18.50	4.6	24.3	16.6	...	...	...	...	12.4	
357.964−0.845	17 44 02.133	−31 06 47.97	10.1	23.3	6.3	9.9	19.1	6.1	−0.8	11.2	
357.965−0.168 e	17 41 21.147	−30 45 22.85	5.1	60.7	27.0	...	...	...	...	12.4	
357.982−0.164 e	17 41 22.546	−30 44 22.99	11.5	131.1	35.3	...	...	...	...	11.5	
357.988−0.159 e	17 41 22.472	−30 43 55.44	8.2	129.3	35.3	...	...	...	...	11.0	
357.993−1.075	17 45 01.281	−31 12 34.75	6.3	5.8	0.0	5.7	8.1	4.5	1.3	10.2	
357.996−0.159 e	17 41 23.429	−30 43 30.74	18.8	286.7	43.3	23.5	835.4	72.3	4.1	10.6	GPSR, Gal
358.002−0.637	17 43 17.924	−30 58 19.07	321.8	342.9	1.8	315.4	348.1	2.3	0.1	24.6	GPSR, xgal
358.007−0.155 e	17 41 24.165	−30 42 50.84	4.1	51.6	26.6	...	...	...	...	10.0	
358.044−0.832 m	17 44 10.560	−31 02 17.70	6.7	6.1	0.8	12.4	19.6	5.4	−0.2	14.7	
358.045−0.833 m	17 44 10.881	−31 02 18.45	5.9	14.3	1.5	...	...	...	...	14.6	
358.053−0.066	17 41 09.863	−30 37 40.43	11.9	20.7	5.3	9.3	23.4	11.7	0.5	5.0	
358.064+0.103	17 40 31.656	−30 31 44.72	20.1	39.4	6.0	17.4	35.2	9.0	−0.4	11.4	
358.083−0.155 e	17 41 35.571	−30 38 58.02	4.2	32.8	22.1	...	...	...	...	7.6	
358.117+0.007	17 41 02.054	−30 32 06.91	11.3	29.7	9.0	11.8	47.7	13.9	1.8	3.8	
358.154+0.027 m	17 41 02.724	−30 29 34.66	12.1	20.1	0.3	12.8	17.2	0.7	...	4.9	
358.157+0.029 m	17 41 02.910	−30 29 22.11	65.2	74.8	0.1	74.8	80.3	0.2	0.1	5.1	GPSR, 1LC
358.186−0.039	17 41 23.061	−30 30 02.51	10.8	10.8	0.0	9.6	15.3	7.1	1.4	3.3	GPSR
358.265−0.140	17 41 58.673	−30 29 13.42	5.3	5.2	0.0	7.0	6.8	0.0	1.0	11.1	
358.266+0.038	17 41 16.725	−30 23 29.84	22.3	27.2	3.4	25.9	29.6	0.0	0.3	9.5	GPSR
358.301+0.141	17 40 57.550	−30 18 25.82	5.3	33.8	14.2	...	...	...	...	15.4	
358.306+0.074	17 41 14.187	−30 20 22.07	23.1	29.8	3.9	20.2	24.5	4.0	−0.8	12.7	
358.325−0.198	17 42 21.062	−30 28 00.43	12.8	15.0	2.6	...	...	...	...	16.8	
358.439−0.211	17 42 41.059	−30 22 36.02	36.2	47.5	4.2	45.1	46.3	0.0	−0.1	17.1	GPSR

TABLE 3—*Continued*

Name (1)	RA (2)	Dec (3)	1658 MHz			1281 MHz			$\alpha$ (10)	$\Theta$ (11)	Notes (12)
			$I$ (4)	$S$ (5)	$\theta$ (6)	$I$ (7)	$S$ (8)	$\theta$ (9)			
358.592+0.046	17 42 02.720	−30 06 41.45	87.5	96.8	2.1	109.6	122.8	2.6	0.9	7.9	GPSR
358.600−0.059 m	17 42 28.556	−30 09 33.72	15.0	23.0	0.5	24.9	57.3	7.6	1.0	4.2	GPSR
358.600−0.060 m	17 42 28.842	−30 09 35.59	10.2	21.7	0.9	...	...	...	...	4.2	
358.609−0.038	17 42 24.990	−30 08 27.12	4.1	5.0	2.2	8.2	17.6	8.1	4.9	3.6	
358.615−0.035	17 42 25.025	−30 08 02.41	8.4	8.6	0.0	17.6	24.8	4.6	4.1	3.3	
358.632+0.063 e	17 42 04.655	−30 04 04.88	50.0	423.4	42.8	61.0	499.0	48.7	0.6	7.5	GPSR,Gal
358.632−0.122 m	17 42 48.164	−30 09 57.29	1.7	1.1	4.6	5.5	5.8	1.3	...	5.6	
358.632−0.123 m	17 42 48.519	−30 09 56.68	5.2	3.6	3.5	6.3	5.7	1.2	3.5	5.6	
358.640−0.271	17 43 24.616	−30 14 14.56	4.4	3.6	0.0	10.2	10.3	0.0	4.1	15.3	
358.644−0.033 e	17 42 28.975	−30 06 32.15	21.0	359.2	65.1	21.2	330.6	61.8	−0.3	1.5	
358.650−0.077 e	17 42 40.194	−30 07 34.49	6.3	137.1	49.9	7.2	113.4	38.7	−0.7	2.5	
358.683−0.117 e	17 42 54.369	−30 07 10.99	21.9	284.8	58.6	30.7	228.5	35.8	−0.9	5.3	
358.696+0.262	17 41 27.186	−29 54 31.04	23.4	36.5	5.2	27.4	35.2	4.3	−0.1	20.1	
358.706+0.002 e	17 42 29.705	−30 02 15.88	...	...	...	6.0	72.3	30.4	...	3.5	
358.710+0.136	17 41 58.869	−29 57 48.90	9.9	11.6	2.7	11.1	15.9	4.8	1.2	11.8	
358.710+0.499 e	17 40 33.490	−29 46 15.56	5.8	15.7	12.6	7.2	16.6	7.2	0.2	17.2	
358.720+0.009 e	17 42 30.106	−30 01 16.81	7.2	131.4	43.9	7.5	68.1	26.2	−2.5	4.5	GPSR
358.721−0.125 e	17 43 01.817	−30 05 29.79	5.6	155.6	57.4	8.3	247.8	56.5	1.8	7.0	
358.784+0.060 e	17 42 27.397	−29 56 26.62	11.0	89.7	27.5	13.6	199.2	36.1	3.1	9.3	
358.784+0.062 e	17 42 26.911	−29 56 23.04	8.4	63.6	25.0	9.9	136.1	37.5	2.9	9.4	
358.787+0.055	17 42 29.139	−29 56 25.26	2.2	2.0	0.0	5.9	7.7	0.0	5.2	9.3	
358.803−0.011 e	17 42 46.951	−29 57 43.05	22.7	322.7	63.7	27.0	116.3	27.1	−4.0	8.6	
358.810+0.737	17 39 52.579	−29 33 37.50	3.7	3.8	0.0	3.9	4.0	0.0	0.2	15.8	
358.837+0.678	17 40 10.160	−29 34 06.46	3.0	3.1	0.0	3.0	1.6	0.0	−2.6	11.8	
358.849+0.161 e	17 42 13.166	−29 49 55.82	14.0	25.5	12.0	28.1	48.1	13.5	2.5	16.5	
358.873+0.276	17 41 49.606	−29 45 02.14	12.1	27.2	6.4	17.9	30.1	4.6	0.4	20.6	
358.887+0.654	17 40 23.213	−29 32 19.92	12.8	12.4	0.0	13.5	17.1	3.5	1.2	8.1	GPSR
358.917+0.072	17 42 44.025	−29 49 16.07	320.2	338.3	1.6	449.7	458.1	1.0	1.2	16.6	GPSR,xgal
358.969+0.796	17 40 01.971	−29 23 38.16	7.4	8.9	2.3	5.2	5.9	2.7	−1.6	14.4	
358.982+0.436 m	17 41 28.098	−29 34 27.53	2.6	10.4	1.9	3.5	15.9	11.1	0.0	9.7	
358.983+0.433 m	17 41 28.970	−29 34 28.87	1.4	5.4	1.1	...	...	...	...	9.9	GPSR,1LC,xgal
358.983+0.580	17 40 54.537	−29 29 49.86	91.0	91.8	0.0	108.5	111.8	1.6	0.8	0.1	
359.073+0.735	17 40 31.391	−29 20 19.32	4.9	5.3	1.4	4.3	4.3	0.0	−0.8	11.1	
359.076+0.547	17 41 15.864	−29 26 06.49	2.5	2.7	1.3	2.9	2.9	0.0	0.3	6.6	
359.088+0.426	17 41 45.811	−29 29 19.26	4.8	5.0	1.0	4.0	3.6	0.0	−1.3	13.0	
359.259+0.749	17 40 55.273	−29 10 25.07	33.5	36.5	0.0	31.6	39.4	4.3	0.3	19.4	GPSR
359.388+0.460	17 42 21.497	−29 12 59.46	57.5	60.6	0.0	72.8	155.8	7.1	3.7	27.6	
359.826+0.029 e	17 45 05.374	−29 04 09.00	27.8	132.3	16.4	...	...	...	...	10.1	Sgr A
359.848−0.015 e	17 45 18.793	−29 04 24.83	33.9	833.0	39.7	...	...	...	...	12.9	Sgr A
359.860−0.074 e	17 45 34.575	−29 05 39.08	58.8	1861.3	53.1	...	...	...	...	16.9	Sgr A
359.864−0.051 e	17 45 29.534	−29 04 44.47	...	...	...	35.0	430.1	32.7	...	11.5	Sgr A
359.868+0.182 m	17 44 35.736	−28 57 12.14	...	...	...	0.7	0.7	0.0	...	0.3	
359.872+0.178 m	17 44 37.075	−28 57 09.22	66.8	83.1	0.0	65.6	81.2	0.0	−0.1	0.3	GPSR,1LC
359.875−0.170	17 45 59.146	−29 07 51.41	96.8	248.9	6.2	...	...	...	...	23.4	Sgr A

TABLE 3—*Continued*

Name (1)	RA (2)	Dec (3)	1658 MHz			1281 MHz			$\alpha$ (10)	$\Theta$ (11)	Notes (12)
			$I$ (4)	$S$ (5)	$\theta$ (6)	$I$ (7)	$S$ (8)	$\theta$ (9)			
359.888−0.086 e	17 45 41.131	−29 04 36.43	...	...	...	65.2	1243.5	46.5	...	11.3	Sgr A
359.897−0.067	17 45 38.110	−29 03 31.65	80.2	264.4	7.9	...	...	...	...	16.8	Sgr A
359.901−0.073 e	17 45 40.020	−29 03 29.42	45.4	959.1	46.7	...	...	...	...	10.2	Sgr A
359.907−0.110 e	17 45 49.562	−29 04 23.74	63.6	2474.0	67.8	...	...	...	...	19.8	Sgr A
359.911−0.074 e	17 45 41.741	−29 03 3.27	22.0	51.5	12.3	...	...	...	...	9.8	Sgr A
359.912−0.069 e	17 45 40.598	−29 02 50.49	31.1	149.7	19.4	...	...	...	...	9.6	Sgr A
359.912−0.160 e	17 46 1.984	−29 05 41.47	40.1	365.4	28.2	...	...	...	...	14.0	Sgr A
359.921−0.065 e	17 45 41.082	−29 02 15.20	75.0	975.9	39.4	...	...	...	...	9.0	Sgr A
359.923−0.013 e	17 45 29.085	−29 00 32.67	31.7	465.9	36.6	...	...	...	...	7.4	Sgr A
359.925−0.093 m	17 45 48.091	−29 02 55.48	...	...	...	49.3	49.3	0.0	...	10.1	Sgr A
359.929−0.094 m	17 45 48.957	−29 02 43.55	...	...	...	33.3	161.7	1.5	...	9.9	Sgr A
359.927−0.055	17 45 39.720	−29 01 37.15	...	...	...	57.1	86.5	5.1	...	8.3	Sgr A
359.928+0.047 e	17 45 15.731	−28 58 23.66	18.7	48.2	10.5	...	...	...	...	10.0	Sgr A
359.929−0.008 e	17 45 28.872	−29 00 3.24	...	...	...	39.8	392.7	29.5	...	7.0	Sgr A
359.930−0.875	17 48 52.992	−29 26 57.92	21.8	148.0	12.1	11.4	156.3	25.2	0.2	19.4	GPSP
359.934−0.058 e	17 45 41.373	−29 01 22.07	23.5	54.8	12.4	...	...	...	...	8.1	Sgr A
359.944−0.047	17 45 40.021	−29 00 29.54	567.2	968.6	4.9	619.4	966.8	5.8	0.0	16.3	GPSP,Sgr *,Gal
359.944−0.104 e	17 45 53.467	−29 02 18.41	40.7	272.5	25.7	...	...	...	...	10.0	Sgr A
359.955−0.117	17 45 58.096	−29 02 9.53	...	...	...	46.9	127.7	8.5	...	10.4	Sgr A
359.955−0.550	17 47 39.813	−29 15 35.50	10.0	24.1	7.5	7.1	127.2	26.1	6.4	18.8	Sgr A
359.966−0.027	17 45 38.617	−28 58 46.11	...	...	...	40.6	80.1	8.2	...	5.5	Sgr A
359.966−0.071 e	17 45 48.997	−29 00 8.87	45.6	743.9	36.6	...	...	...	...	7.5	Sgr A
359.972−0.100 e	17 45 56.472	−29 00 42.97	53.2	1062.3	42.2	...	...	...	...	20.4	Sgr A
359.978−0.056 e	17 45 46.962	−28 59 4.04	...	...	...	70.6	1603.2	50.5	...	6.4	Sgr A
359.981−0.049 e	17 45 45.851	−28 58 38.72	38.1	180.1	21.6	...	...	...	...	5.9	Sgr A
359.985+0.027	17 45 28.666	−28 56 4.11	36.8	64.3	4.5	25.2	40.4	5.2	−1.8	3.3	Sgr A
359.985+0.027	17 45 28.667	−28 56 06.90	59.3	128.9	5.3	...	...	...	...	13.2	Sgr A
359.991−0.011 e	17 45 38.345	−28 56 58.57	...	...	...	68.6	1663.8	54.5	...	3.7	Sgr A
359.994−0.051 e	17 45 48.126	−28 58 04.85	70.5	3999.4	78.8	...	...	...	...	18.1	Sgr A
359.998−0.016 e	17 45 40.638	−28 56 44.85	15.9	20.9	8.9	...	...	...	...	3.6	Sgr A
0.005−0.891	17 49 07.229	−29 23 35.64	47.3	128.2	7.0	79.0	209.9	8.0	1.9	16.7	GPSP
0.012+0.007 e	17 45 37.020	−28 55 20.04	28.8	93.0	13.3	...	...	...	...	15.4	Sgr A
0.012−0.087 e	17 45 59.338	−28 58 16.62	...	...	...	39.8	346.2	29.4	...	7.6	Sgr A
0.018−0.093 e	17 46 1.373	−28 58 9.48	...	...	...	24.1	128.4	18.0	...	8.0	Sgr A
0.027−0.023	17 45 46.374	−28 55 29.51	...	...	...	17.5	22.1	3.5	...	3.4	Arch
0.029+0.021	17 45 36.280	−28 53 59.07	...	...	...	32.5	40.0	3.3	...	0.7	Arch
0.034+0.013 e	17 45 38.827	−28 53 59.73	52.0	1142.0	41.1	...	...	...	...	16.0	Sgr A
0.047−0.065 e	17 45 59.025	−28 55 45.78	...	...	...	51.5	166.7	17.4	...	6.2	Arch
0.056−0.041 e	17 45 54.668	−28 54 32.99	48.4	243.2	16.6	...	...	...	...	19.8	Sgr A
0.061+0.026 e	17 45 39.821	−28 52 14.85	42.2	408.1	35.1	...	...	...	...	16.7	Sgr A
0.061−0.062 e	17 46 0.320	−28 54 58.33	...	...	...	37.2	205.8	22.6	...	6.3	Arch



TABLE 3—*Continued*

Name (1)	RA (2)	Dec (3)	1658 MHz			1281 MHz			$\alpha$ (10)	$\Theta$ (11)	Notes (12)
			$I$ (4)	$S$ (5)	$\theta$ (6)	$I$ (7)	$S$ (8)	$\theta$ (9)			
0.061–0.000 e	17 45 45.863	–28 53 3.13	...	...	...	13.9	19.3	8.5	...	2.5	Arch
0.069+0.040 e	17 45 37.645	–28 51 21.97	23.7	136.7	21.3	...	...	...	...	2.0	Arch
0.069–0.025 e	17 45 52.983	–28 53 24.62	38.8	139.8	16.8	...	...	...	...	4.2	Arch
0.083–0.614	17 48 13.003	–29 11 02.62	...	...	...	5.3	85.2	31.5	...	9.4	
0.084–0.931	17 49 28.055	–29 20 46.38	16.4	19.7	3.1	14.7	75.5	12.1	5.2	16.5	GPSR
0.085–0.613	17 48 12.989	–29 10 53.43	7.7	42.4	11.6	...	...	...	...	9.3	
0.092–0.075 e	17 46 07.826	–28 53 46.76	92.8	287.0	13.7	...	...	...	...	23.2	Sgr A
0.097–0.057 e	17 46 4.167	–28 52 57.93	22.0	181.1	24.4	...	...	...	...	7.1	Arch
0.099+0.089 e	17 45 30.458	–28 48 19.55	33.7	393.6	30.9	...	...	...	...	5.2	Arch
0.101+0.080 e	17 45 32.975	–28 48 29.79	24.1	120.4	20.1	...	...	...	...	4.9	Arch
0.102+0.025 e	17 45 45.850	–28 50 11.91	35.6	98.6	14.3	...	...	...	...	4.0	Arch
0.112–0.130 e	17 46 23.349	–28 54 29.45	230.0	2363.5	0.0	...	...	...	...	27.0	Sgr A
0.115+0.083 e	17 45 34.054	–28 47 39.43	20.8	75.9	15.5	...	...	...	...	5.7	Arch
0.117–0.001 e	17 45 54.064	–28 50 14.58	27.8	197.3	23.3	...	...	...	...	5.5	Arch
0.139+0.100 e	17 45 33.541	–28 45 54.36	29.4	159.0	20.9	...	...	...	...	7.5	Arch
0.142–0.034 e	17 46 5.238	–28 49 57.44	31.0	264.3	26.5	...	...	...	...	8.1	Arch
0.153+0.113 e	17 45 32.604	–28 44 49.44	34.8	655.1	42.5	...	...	...	...	8.6	Arch
0.192–0.687	17 48 45.703	–29 07 39.05	47.0	55.3	2.3	37.1	44.3	3.0	–0.9	0.6	
0.196–0.069 e	17 46 21.081	–28 48 16.09	23.5	402.4	34.6	...	...	...	...	12.4	Arch
0.198–0.033 e	17 46 13.007	–28 47 1.95	...	...	...	58.9	1052.0	43.4	...	11.2	Arch
0.206+0.151 e	17 45 31.250	–28 40 54.22	86.5	2424.1	45.4	...	...	...	...	21.3	Sgr A
0.217+0.079 e	17 45 49.447	–28 42 35.66	57.2	350.4	26.8	...	...	...	...	11.3	Arch
0.235+0.168 e	17 45 31.348	–28 38 52.91	102.6	3182.1	50.4	...	...	...	...	22.9	Sgr A
0.280–0.483	17 48 10.281	–28 56 51.16	37.5	218.7	10.7	46.6	202.8	10.6	–0.3	14.3	
0.305+0.394	17 44 48.801	–28 28 13.04	9.6	9.4	0.0	11.7	12.8	0.0	1.2	17.6	
0.318–0.388 m	17 47 53.205	–28 51 54.68	...	...	...	11.1	12.0	17.4	...	20.9	
0.321–0.389 m	17 47 53.992	–28 51 49.25	...	...	...	5.4	31.4	9.5	...	20.8	
0.334–0.494	17 48 20.337	–28 54 24.26	17.2	128.8	12.3	13.2	20.0	5.3	–7.2	14.9	
0.337–0.706	17 49 10.711	–29 00 47.45	8.8	69.0	12.4	7.2	3.8	0.0	–11.2	8.9	
0.380+0.019 e	17 46 26.957	–28 36 06.01	28.8	675.4	44.5	56.3	927.8	69.7	1.2	18.0	
0.384+0.000 e	17 46 31.818	–28 36 28.37	...	...	...	6.6	106.9	44.5	...	18.9	

TABLE 3—*Continued*

Name (1)	RA (2)	Dec (3)	1658 MHz			1281 MHz			$\alpha$ (10)	$\Theta$ (11)	Notes (12)
			$I$ (4)	$S$ (5)	$\theta$ (6)	$I$ (7)	$S$ (8)	$\theta$ (9)			
0.391+0.231	17 45 38.858	−28 28 54.10	...	...	...	6.1	6.9	2.2	...	9.1	GPSR
0.419+0.116 e	17 46 09.659	−28 31 02.51	5.1	148.7	52.4	...	...	...	...	11.5	
0.432+0.261	17 45 37.615	−28 25 53.63	12.9	14.5	1.7	10.1	11.1	2.1	−1.0	6.6	
0.440+0.587 m	17 44 23.035	−28 15 16.25	9.3	13.5	3.4	14.4	24.1	2.1	5.6	22.8	
0.450+0.592 m	17 44 23.338	−28 14 38.02	...	...	...	8.5	32.8	14.8	...	22.9	
0.458−0.075	17 46 59.840	−28 35 01.87	...	...	...	37.7	130.2	11.3	...	22.4	
0.461−0.071	17 46 59.350	−28 34 44.59	...	...	...	21.4	42.4	9.3	...	22.1	
0.463+0.143 e	17 46 09.720	−28 27 59.42	5.2	211.6	57.4	...	...	...	...	8.8	
0.467−0.069 e	17 46 59.753	−28 34 23.97	...	...	...	17.2	19.2	7.0	...	22.0	
0.470−0.055	17 46 56.889	−28 33 45.96	35.3	80.4	5.1	47.1	114.9	14.0	1.4	21.0	
0.487−0.701	17 49 30.557	−28 52 56.58	13.7	33.9	7.0	18.9	36.5	6.9	0.3	18.1	
0.489−0.057 e	17 46 59.935	−28 32 53.51	34.3	151.7	18.0	31.9	119.4	14.8	−0.9	21.1	
0.490−0.073	17 47 03.972	−28 33 18.24	...	...	...	47.6	159.8	9.8	...	22.1	
0.491+0.194 e	17 46 01.562	−28 24 57.88	...	...	...	12.3	143.3	31.7	...	5.1	
0.491−0.777	17 49 48.967	−28 55 04.93	15.0	57.3	9.5	10.8	65.7	14.8	0.5	19.7	
0.492+0.157 e	17 46 10.428	−28 26 03.48	7.5	127.6	44.4	...	...	...	...	7.3	
0.495−0.069	17 47 03.735	−28 32 55.69	...	...	...	14.9	21.4	5.3	...	21.9	
0.498−0.047 e	17 46 58.931	−28 32 06.88	...	...	...	28.7	55.2	10.2	...	20.4	
0.507+0.051 e	17 46 37.348	−28 28 37.20	4.9	30.6	23.2	...	...	...	...	14.0	
0.510−0.037	17 46 58.223	−28 31 09.93	23.0	77.1	7.7	16.2	13.9	6.0	−6.6	19.7	
0.510+0.093	17 46 28.104	−28 27 07.92	2.2	12.2	9.4	...	...	...	...	11.2	
0.510+0.167 e	17 46 10.651	−28 24 50.82	2.9	16.0	0.0	...	...	...	...	6.4	
0.511+0.272	17 45 46.371	−28 21 30.39	1.0	1.0	0.0	...	...	...	...	1.8	
0.512−0.038 e	17 46 58.819	−28 31 04.68	20.0	35.2	9.7	16.2	13.9	6.0	−3.6	19.8	
0.517−0.027	17 46 56.831	−28 30 30.80	...	...	...	10.4	28.4	11.3	...	19.1	
0.517−0.033 e	17 46 58.249	−28 30 42.53	...	...	...	17.2	1.8	2.3	...	19.5	
0.522−0.096 e	17 47 13.763	−28 32 23.49	...	...	...	25.0	36.0	8.6	...	23.7	
0.527+0.181	17 46 09.880	−28 23 30.47	31.4	29.6	0.0	15.2	17.7	10.1	−2.0	5.4	
0.528+0.181 e	17 46 10.046	−28 23 29.75	82.1	392.1	30.5	108.4	351.5	20.5	−0.4	5.5	
0.528−0.029 e	17 46 59.014	−28 29 58.86	...	...	...	27.6	81.6	13.1	...	19.3	
0.531+0.131	17 46 22.103	−28 24 52.12	2.0	2.3	0.0	...	...	...	...	8.7	GPSR,1LC
0.538+0.262	17 45 52.500	−28 20 26.41	86.3	88.3	0.7	63.6	64.8	0.0	−1.2	0.1	
0.545+0.073 e	17 46 37.634	−28 25 58.51	7.0	176.7	53.1	...	...	...	...	12.7	
0.547−0.849 e	17 50 13.960	−28 54 23.20	80.0	765.7	26.5	54.7	194.9	1.1	−2.3	25.2	
0.552+0.074	17 46 38.406	−28 25 32.34	...	...	...	9.9	14.8	4.5	...	12.7	
0.558+0.241	17 46 00.356	−28 20 01.95	2.1	2.5	2.5	...	...	...	...	2.1	

TABLE 3—*Continued*

Name (1)	RA (2)	Dec (3)	1658 MHz			1281 MHz			$\alpha$ (10)	$\Theta$ (11)	Notes (12)
			$I$ (4)	$S$ (5)	$\theta$ (6)	$I$ (7)	$S$ (8)	$\theta$ (9)			
0.560−0.116 e	17 47 23.825	−28 31 05.62	77.4	1507.1	51.6	...	...	...	...	25.3	GPSR
0.561+0.244 m	17 46 00.008	−28 19 49.36	1.8	5.0	5.7	...	...	...	...	2.1	
0.561+0.277 m	17 45 52.303	−28 18 45.70	1.2	1.2	0.0	...	...	...	...	1.7	
0.561+0.278 m	17 45 52.167	−28 18 44.80	1.2	1.2	0.0	...	...	...	...	1.7	
0.562+0.240 m	17 46 00.993	−28 19 53.82	2.5	8.7	7.3	...	...	...	...	2.3	
0.562−0.818	17 50 08.596	−28 52 40.36	14.3	33.1	5.6	24.2	17.3	0.0	−2.5	25.1	
0.563+0.242 m	17 46 00.676	−28 19 46.43	3.5	13.4	7.3	...	...	...	...	2.3	
0.562+0.246 m	17 45 59.798	−28 19 41.18	2.5	8.0	6.3	...	...	...	...	2.1	
0.598−0.052	17 47 14.262	−28 27 07.98	...	...	...	17.9	22.6	3.5	...	21.6	
0.600−0.048 m	17 47 13.729	−28 26 53.85	85.5	183.3	5.3	134.5	463.1	0.7	...	21.4	GPSR, Gal
0.603−0.051 m	17 47 14.646	−28 26 51.52	158.2	338.0	4.7	159.9	272.9	5.0	1.2	21.6	
0.601−0.037	17 47 11.198	−28 26 31.82	36.5	50.9	3.3	14.6	25.7	6.0	−2.6	20.7	
0.605−0.052 m	17 47 15.241	−28 26 44.39	15.6	20.1	2.4	...	...	...	...	21.7	
0.606+0.018 m	17 46 59.032	−28 24 31.63	...	...	...	8.1	18.7	1.5	...	17.3	
0.608+0.021 m	17 46 58.740	−28 24 22.61	...	...	...	4.9	8.3	1.9	...	17.1	
0.621−0.063 m	17 47 19.994	−28 26 17.38	...	...	...	17.2	36.2	2.6	...	22.8	
0.623−0.061 m	17 47 20.055	−28 26 07.40	...	...	...	13.6	24.0	1.4	...	22.7	
0.625+0.110 m	17 46 40.257	−28 20 40.91	1.3	4.6	7.7	...	...	...	...	12.1	
0.626+0.108 m	17 46 40.840	−28 20 42.48	0.6	1.4	5.6	...	...	...	...	12.2	
0.628+0.111 m	17 46 40.537	−28 20 33.46	−0.5	−4.6	13.2	...	...	...	...	12.1	
0.629+0.111 m	17 46 40.714	−28 20 29.30	2.6	40.1	19.6	...	...	...	...	12.2	
0.629−0.028 e	17 47 13.183	−28 24 46.53	...	...	...	154.5	913.1	23.8	...	20.8	GPSR, Gal
0.630−0.029 e	17 47 13.363	−28 24 44.61	108.2	1326.2	34.5	...	...	...	...	20.8	
0.635−0.020	17 47 12.141	−28 24 14.33	6.2	6.7	0.0	...	...	...	...	20.4	
0.641−0.059	17 47 21.999	−28 25 09.78	68.2	330.8	11.8	...	...	...	...	23.0	
0.642−0.053 e	17 47 20.717	−28 24 56.11	...	...	...	90.4	2061.3	48.5	...	22.6	

TABLE 3—*Continued*

Name (1)	RA (2)	Dec (3)	1658 MHz			1281 MHz			$\alpha$ (10)	$\Theta$ (11)	Notes (12)
			$I$ (4)	$S$ (5)	$\theta$ (6)	$I$ (7)	$S$ (8)	$\theta$ (9)			
0.643−0.051 m	17 47 20.295	−28 24 48.36	22.0	40.8	6.1	54.8	82.2	5.7	−2.3	22.5	
0.644−0.053 m	17 47 20.931	−28 24 48.20	24.8	56.9	6.5	...	...	...	...	22.7	
0.644−0.055 m	17 47 21.473	−28 24 52.16	22.5	51.2	6.6	...	...	...	...	22.8	
0.644−0.047 e	17 47 19.660	−28 24 38.09	43.8	151.2	15.7	19.8	24.5	4.0	−7.1	22.3	
0.658−0.042	17 47 20.443	−28 23 44.73	146.7	195.7	2.9	47.9	70.0	5.8	−4.0	22.4	
0.659−0.006	17 47 12.135	−28 22 34.40	63.5	165.9	6.6	96.2	297.4	17.2	2.3	20.1	
0.661−0.045	17 47 21.409	−28 23 40.99	17.2	46.1	7.7	47.9	70.0	5.8	1.6	22.6	
0.663−0.042	17 47 21.157	−28 23 27.68	28.6	49.9	5.8	...	...	...	...	22.5	
0.664−0.005 e	17 47 12.583	−28 22 16.07	...	...	...	16.8	7.4	4.3	...	20.2	
0.667−0.035 e	17 47 20.169	−28 23 03.78	264.0	3097.2	41.4	291.8	2869.9	38.2	−0.3	22.2	
0.680−0.028 e	17 47 20.312	−28 22 12.15	251.3	2442.8	30.9	265.4	1606.5	22.5	−1.6	22.1	
0.683−0.035 e	17 47 22.181	−28 22 14.20	30.2	107.3	15.0	53.6	142.8	8.1	1.1	22.6	
0.689−0.033	17 47 22.632	−28 21 53.88	110.3	207.6	4.8	127.5	228.0	6.8	0.4	22.7	
0.693−0.045	17 47 26.148	−28 22 03.62	94.1	256.9	7.0	121.4	314.1	0.9	2.3	23.6	
0.722+0.406	17 45 45.139	−28 06 29.24	5.8	8.9	0.0	7.2	10.2	0.0	0.5	14.0	
0.815+1.700	17 40 59.644	−27 21 01.12	14.7	19.5	3.3	22.1	23.2	1.5	0.7	17.6	GPSR
0.832+1.591	17 41 27.095	−27 23 34.42	2.5	3.4	3.5	2.7	3.2	0.0	−0.2	13.6	
0.846+1.173	17 43 05.441	−27 36 04.65	...	...	...	136.1	168.5	3.5	...	27.5	GPSR
0.858+1.840	17 40 33.794	−27 14 22.98	13.2	31.6	9.4	26.7	155.7	23.5	6.2	22.3	
0.936+1.471	17 42 09.574	−27 22 05.86	9.0	9.2	0.0	13.2	14.3	2.1	1.7	8.9	
0.952+1.515	17 42 01.848	−27 19 52.15	17.5	17.0	0.0	18.6	19.1	1.2	0.5	6.5	GPSR
0.971+1.787	17 41 02.060	−27 10 16.36	5.5	27.8	11.7	11.6	27.3	8.7	−0.1	15.5	GPSR
1.011+0.027	17 47 54.008	−28 03 29.55	25.4	28.3	5.8	32.3	63.9	9.7	3.2	12.6	
1.012+1.283	17 43 03.642	−27 24 08.88	3.9	3.4	0.0	6.2	6.9	0.0	2.7	18.6	
1.026+1.351	17 42 49.855	−27 21 18.65	10.3	16.1	4.3	10.9	14.9	4.5	−0.3	14.1	GPSR
1.035+1.559 m	17 42 03.450	−27 14 13.80	2.1	2.1	0.0	1.9	2.2	0.0	0.9	0.9	GPSR
1.026+1.545 m	17 42 05.310	−27 15 11.40	7.5	52.2	0.0	13.9	70.4	0.0	...	1.9	
1.048+1.573 m	17 42 01.947	−27 13 09.70	118.3	153.2	3.3	156.4	189.9	3.5	...	0.3	
1.031+1.661	17 41 39.596	−27 11 15.15	2.9	4.6	4.0	3.3	3.2	0.0	−1.4	6.2	
1.048+0.055	17 47 52.871	−28 00 42.84	14.0	22.2	4.4	...	...	...	...	11.1	
1.081+1.461 m	17 42 32.522	−27 15 02.96	3.0	6.3	6.0	4.6	15.3	0.8	...	7.6	
1.082+1.464 m	17 42 32.022	−27 14 53.74	2.4	7.0	7.1	...	...	...	...	7.4	
1.085+1.468 m	17 42 31.387	−27 14 35.37	7.5	18.1	8.6	12.7	12.7	0.0	−0.4	7.2	GPSR
1.113+1.664 m	17 41 50.459	−27 06 57.31	2.7	4.8	4.8	...	...	...	...	7.2	
1.113+1.667 m	17 41 49.889	−27 06 53.76	2.8	4.6	4.5	5.6	11.0	1.5	0.4	7.3	
1.114+1.666 m	17 41 50.054	−27 06 51.24	2.3	3.4	4.5	...	...	...	...	7.3	
1.115+1.664 m	17 41 50.811	−27 06 53.80	4.1	7.2	5.9	6.2	11.2	1.6	...	7.2	
1.127+1.328 m	17 43 09.565	−27 16 50.36	2.9	3.6	0.0	4.9	4.2	0.0	...	17.0	
1.130+1.324 m	17 43 10.999	−27 16 49.61	3.0	3.2	0.0	3.2	2.9	0.0	...	17.3	
1.133+1.320 m	17 43 12.177	−27 16 48.09	9.5	17.3	5.6	15.3	20.3	3.6	0.5	17.6	
1.127−0.106	17 48 41.421	−28 01 39.59	151.5	1643.7	22.6	173.6	1837.3	25.8	0.4	7.2	

TABLE 3—*Continued*

Name (1)	RA (2)	Dec (3)	1658 MHz			1281 MHz			$\alpha$ (10)	$\Theta$ (11)	Notes (12)
			$I$ (4)	$S$ (5)	$\theta$ (6)	$I$ (7)	$S$ (8)	$\theta$ (9)			
1.167+0.053	17 48 10.035	−27 54 40.76	18.9	58.8	9.5	17.3	15.5	6.2	−5.2	5.2	
1.226+0.028	17 48 24.081	−27 52 24.96	8.2	8.3	0.0	...	...	...	...	3.1	
1.285−0.055	17 48 51.518	−27 51 57.29	34.6	54.2	6.3	37.6	82.3	9.3	1.6	6.0	GPSR
1.360+1.579 m	17 42 44.861	−26 57 03.82	8.2	8.4	0.0	10.6	11.1	0.0	2.2	19.4	GPSR
1.361+1.579 m	17 42 45.272	−26 56 59.91	...	...	...	2.0	1.9	0.0	...	19.5	
1.361+1.580 m	17 42 44.951	−26 56 57.60	...	...	...	1.8	1.7	0.0	...	19.5	
3.565+0.577	17 51 40.089	−25 35 04.38	2.4	2.4	0.0	...	...	...	...	11.4	
3.631+0.684	17 51 24.430	−25 28 22.85	1.2	1.2	0.0	...	...	...	...	8.0	
3.690+0.512 e	17 52 11.977	−25 30 35.49	6.7	64.0	34.6	10.0	101.9	34.7	1.8	8.4	
3.703+0.796 e	17 51 08.634	−25 21 14.38	10.0	65.9	30.1	13.7	95.2	34.8	1.4	11.0	
3.714+0.763	17 51 17.623	−25 21 39.36	1.6	1.6	0.0	...	...	...	...	8.7	
3.724+0.546 e	17 52 08.628	−25 27 45.33	4.7	26.1	23.0	5.6	27.8	22.5	0.2	5.7	
3.735+0.679	17 51 39.827	−25 23 10.98	2.6	2.6	0.0	2.5	2.5	0.0	−0.2	3.0	
3.742+0.920	17 50 45.649	−25 15 24.76	47.0	49.1	1.0	48.0	50.3	1.4	0.1	18.5	GPSR
3.745+0.635	17 51 51.265	−25 23 59.80	1020.7	1025.3	0.3	1216.8	1223.2	0.4	0.7	0.0	GPSR,VLA,xgal
3.799+0.590 e	17 52 08.831	−25 22 34.44	1.5	3.5	12.5	...	...	...	...	4.6	
3.807+0.600 e	17 52 07.646	−25 21 52.19	...	...	...	2.2	8.8	18.0	...	4.6	
3.814+0.972 m	17 50 43.650	−25 10 04.26	...	...	...	6.6	8.0	2.3	...	21.9	
3.814+0.974 m	17 50 43.237	−25 10 02.36	...	...	...	5.6	8.3	1.8	...	22.0	
3.826+0.385	17 52 59.347	−25 27 27.16	33.9	50.1	3.0	34.8	49.1	3.3	−0.1	17.4	GPSR,Gal
3.829+0.537	17 52 24.833	−25 22 39.58	6.0	9.7	3.5	5.9	8.6	3.9	−0.5	8.5	
3.929+0.253	17 53 43.389	−25 26 09.17	38.0	70.4	4.6	53.4	68.8	2.9	−0.1	28.1	GPSR

NOTE.—(1) An “e” following a source’s name indicates the source is extended; “m” indicates that a source is one of multiple components. (2) and (3) Right ascension and declination are epoch J2000. (4) and (7) Peak intensities,  $I$ , are in units of mJy beam<sup>−1</sup>, with a 5'' beam. (5) and (8) Integrated fluxes,  $S$ , are in units of mJy. (6) and (9) Apparent sizes,  $\theta$ , are in units of arcseconds. (10) Spectral index defined as  $S \propto \nu^{-\alpha}$  and calculated between 1281 and 1658 Mhz. Extreme values probably reflect the closely spaced observing frequencies. (11) Offset from phase center in arcminutes. (12) Source cross-identifications—“GPSR” indicates the source has a counterpart in the Columbia Galactic plane survey, “ILC” indicates a source also detected in our 6 cm survey, “VLA” indicates VLA calibrators, “Gal” indicates sources likely to be Galactic, and “xgal” indicates sources likely to be extragalactic.

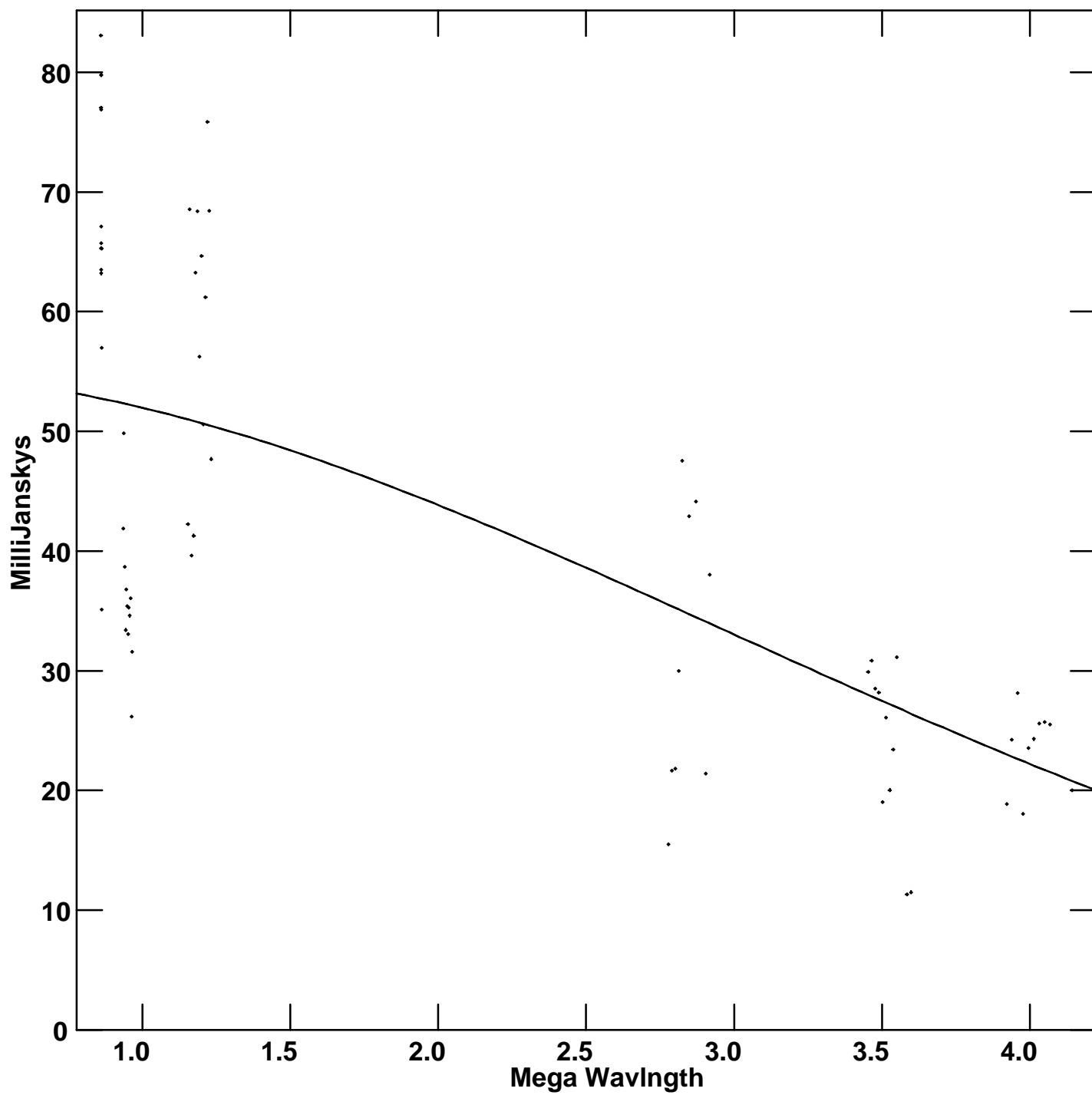
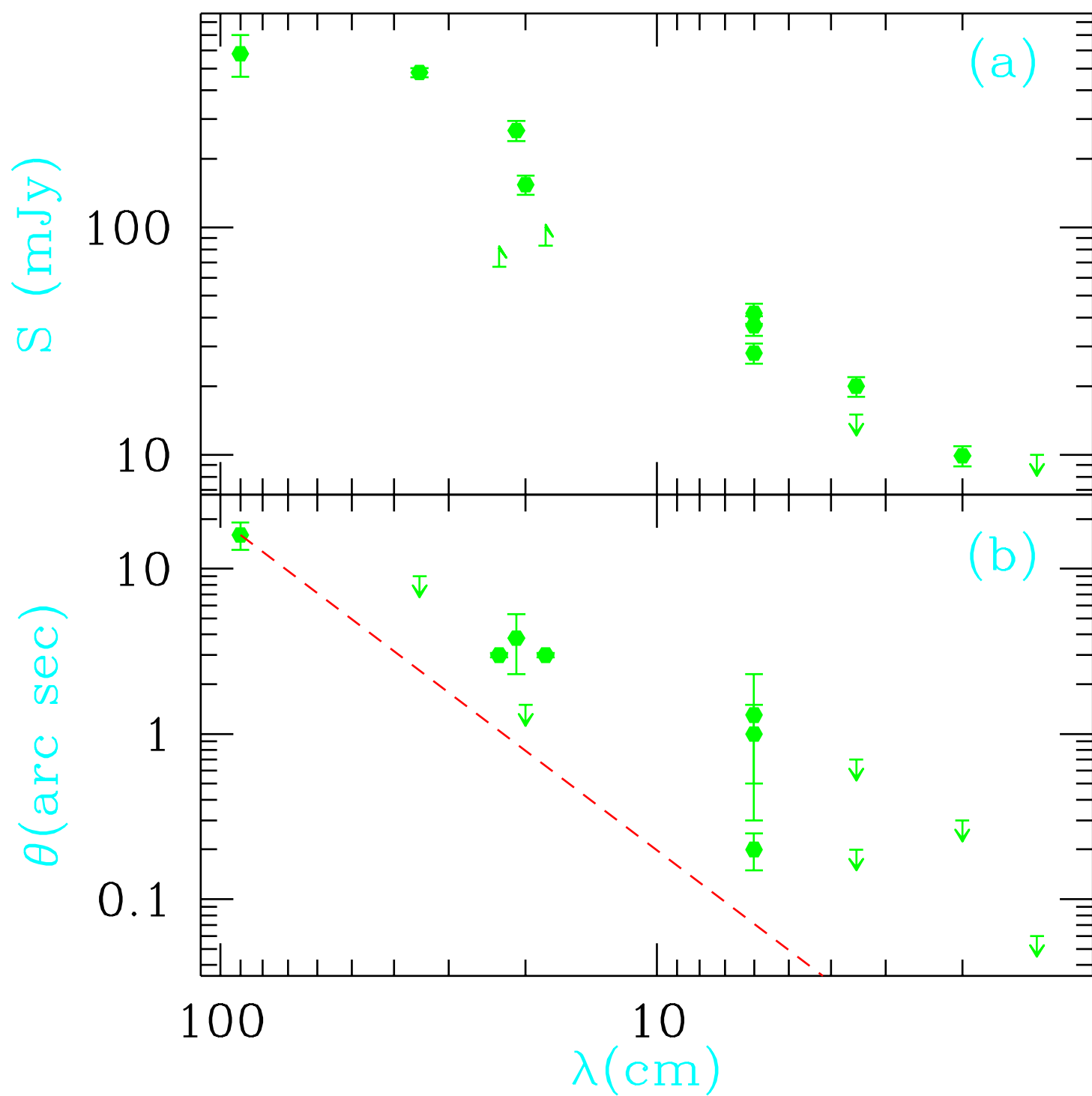


TABLE 4  
SOURCES FROM 1LC 6 CM SURVEY

Name (1)	RA (2)	Dec (3)	$I$ (4)	$S$ (5)	$\theta$ (6)	$\alpha$ (7)	$\Theta$ (8)	Notes (9)
357.865−0.996	17 44 23.588	−31 16 35.89	759.5	777.5	0.0	−0.6	0.0	GPSR
357.901−1.053	17 44 42.364	−31 16 33.92	9.1	9.1	0.0	−0.4	4.7	
358.157+0.029 m	17 41 02.912	−30 29 22.32	6.5	6.8	1.2	...	5.1	GPSR
358.159+0.025 m	17 41 03.919	−30 29 21.95	8.8	17.0	0.6	1.2	4.8	GPSR
358.186−0.039	17 41 23.049	−30 30 02.63	4.5	4.6	0.0	0.9	0.0	GPSR
358.188−0.042 e	17 41 24.055	−30 30 02.55	6.4	37.2	29.8	...	0.3	
358.592+0.046	17 42 02.713	−30 06 41.33	38.3	56.9	1.5	0.5	7.9	
358.600−0.059 e	17 42 28.594	−30 09 35.08	7.3	49.5	17.6	−0.5	4.2	GPSR
358.643−0.034 e	17 42 29.085	−30 06 34.96	9.5	341.7	59.6	0.0	1.6	GPSR
358.968+0.583	17 40 51.596	−29 30 28.79	3.7	3.9	0.0	...	0.9	
358.983+0.580	17 40 54.534	−29 29 49.95	79.8	82.7	0.4	0.2	0.1	GPSR,xgal
358.996+0.582	17 40 55.956	−29 29 03.88	2.8	2.6	0.0	...	0.9	
359.871+0.178 m	17 44 36.853	−28 57 11.42	6.7	8.4	2.9	...	0.2	
359.872+0.178 m	17 44 37.089	−28 57 09.48	36.4	41.9	0.8	0.6	0.3	GPSR
359.973+0.001	17 45 33.041	−28 57 33.67	247.7	230.2	0.0	...	3.0	
0.192−0.687	17 48 45.695	−29 07 39.06	199.1	204.4	0.2	−1.2	0.6	
0.432+0.261	17 45 37.596	−28 25 53.70	38.6	64.4	1.5	−1.4	6.6	
0.525+0.182 e	17 46 09.382	−28 23 35.70	8.8	49.0	18.7	−0.6	5.4	
0.527+0.181 e	17 46 10.004	−28 23 30.87	109.4	1325.6	64.6	−1.1	5.5	
0.538+0.262	17 45 52.492	−28 20 25.92	208.9	221.0	0.0	−0.9	0.1	GPSR
1.026+1.546 m	17 42 05.167	−27 15 08.54	2.1	20.7	28.1	...	1.8	
1.048+1.574 m	17 42 01.914	−27 13 09.45	55.9	68.0	1.3	0.8	0.4	
1.126−0.107 e	17 48 41.453	−28 01 42.22	73.0	3181.6	69.5	−0.5	2.3	GPSR
1.284−0.053 m	17 48 51.061	−27 51 56.06	8.6	29.0	0.9	...	0.0	
1.284−0.055 m	17 48 51.491	−27 51 57.57	15.4	18.1	1.3	...	0.1	GPSR
3.745+0.635	17 51 51.265	−25 23 59.80	475.5	478.9	0.1	0.7	0.0	GPSR,VLA,xgal

NOTE.—(1) An “e” following a source’s name indicates the source is extended; “m” indicates that the source is one of multiple components. (2) and (3) Right ascension and declination are epoch J2000. (4) Peak intensities,  $I$ , are in units of mJy beam<sup>−1</sup>, with a 1′/8 beam. (5) Integrated fluxes,  $S$ , are in units of mJy. (6) Apparent sizes,  $\theta$ , are in units of arcseconds. (7) Spectral index defined as  $S \propto \nu^{-\alpha}$  and taken between 6 and 20 cm. (8) Offset from phase center in arc minutes. (9) Source cross identifications—“GPSR” indicate the source has a counterpart in the Columbia Galactic plane survey, “VLA” indicates VLA calibrators, “Gal” indicates sources likely to be Galactic, and “xgal” indicates sources likely to be extragalactic.





# Hyperstrong Radio-Wave Scattering in the Galactic Center. I. A Survey for Extragalactic Sources Seen Through the Galactic Center

T. Joseph W. Lazio<sup>1</sup>

Naval Research Laboratory, Code 7210, Washington, DC 20375-5351; lazio@rsd.nrl.navy.mil

and

James M. Cordes

Department of Astronomy and National Astronomy & Ionosphere Center,  
Cornell University, Ithaca, NY 14853-6801;  
cordes@spacenet.tn.cornell.edu

## ABSTRACT

The scattering diameters of Sgr A\* and several nearby OH masers ( $\approx 1''$  at 1 GHz) indicate that a region of enhanced scattering is along the line of sight to the Galactic center. The scattering diameter of an extragalactic source seen through this scattering region will be larger by the ratio of the Sun-GC distance to the GC-scattering region separation. This ratio could be a factor of a few, if the scattering region is far from the GC and only a random superposition with it, to more than 100, if the scattering region is within the GC. We have used the VLA to survey 10 (11) fields at 20 cm (6 cm) that are between  $7'$  and  $137'$  from Sgr A\*. Our objective was to identify extragalactic sources and measure their scattering diameters so as to constrain the GC-scattering region separation. In order to find sources within these fields, we have employed pdfCLEAN, a source detection algorithm in which sources are identified in an image by comparing the intensity histogram of the image to that expected from a noise-only image. We found over 100 sources, with the faintest sources being approximately 3 mJy. The average number of sources per field is approximately 10, though fields close to Sgr A\* tend to contain fewer sources. In a companion paper we combine our survey with previous observations of the GC, and we assess the likelihood that the scattering region is so close to the GC that the resulting scattering diameters cause extragalactic sources to be resolved out by our observations.

A number of Galactic sources is included in our source catalog. We discuss the double-lobed source 1LC 359.872+0.178, potentially an X-ray quiet version of 1E 1740.7–2942, a shell-like structure with a central point source, and a possible radio transient.

---

<sup>1</sup>NRC-NRL Research Associate

*Subject headings:* Galaxy:center — ISM:general — scattering — surveys

## 1. Introduction

If viewed through a plasma containing density fluctuations, an otherwise unresolved source will have a visibility, as measured by an interferometer of baseline length  $b$ , of

$$V(b) = \exp \left[ -\frac{1}{2} D_\phi(b) \right]. \quad (1)$$

The phase structure function,  $D_\phi(b) \equiv \langle [\phi(0) - \phi(b)]^2 \rangle$ , is a measure of the phase perturbations, on a length scale  $b$ , imposed on a propagating electromagnetic wave by fluctuations in the electron density.

For a plane wave impinging on this scattering region

$$D_\phi(b) = 8\pi^2 r_e^2 \lambda^2 \int_0^D dz \int_0^\infty dq q [1 - J_0(bq)] P_{\delta n_e}(q, z), \quad (2)$$

where  $r_e$  is the classical electron radius,  $J_0(x)$  is the zeroth-order Bessel function,  $P_{\delta n_e}$  is the spatial spectrum of the density fluctuations, and the integral over  $z$  is taken *from the source to the observer*. If the source of radiation is close to or embedded within the scattering medium, so that the medium is illuminated by spherical wavefronts, the argument of the Bessel function is  $bq(z/D)$  (Ishimaru 1978); the factor  $z/D$  accounts for the divergence of spherical waves.

The apparent angular diameter of the source is determined by the width of the visibility function, and, hence, by how quickly  $D_\phi(b)$  decreases as a function of  $b$ . Since  $z/D < 1$ , the difference in the form of the phase structure function for plane and spherical wavefronts means that sources close to the medium will show smaller angular diameters than those far from it. Hence, by comparing the scattering diameters of Galactic and extragalactic sources along similar lines of sight, one can constrain the *radial* location of the scattering material.

Toward the Galactic center, the observed diameter of Sgr A\* scales as  $\lambda^2$  over the wavelength range 30 cm to 3 mm (Davies, Walsh, & Booth 1976; Rogers et al. 1994), as expected if very strong interstellar scattering from microstructure in the electron density determines the observed diameter. Maser spots in OH/IR stars within 25' of Sgr A\* also show enhanced angular broadening (van Langevelde et al. 1992; Frail et al. 1994). The scattering disks of Sgr A\* and many of the OH masers are observed to be anisotropic as well (van Langevelde et al. 1992; Backer et al. 1993; Krichbaum et al. 1993; Frail et al. 1994; Yusef-Zadeh et al. 1994); in the case of Sgr A\*, its scattering disk is anisotropic at least over the wavelength range 21 cm to 7 mm. These observations indicate that a region of enhanced scattering with an angular extent of at least 25' (60 pc at 8.5 kpc) is along the line of sight to Sgr A\*. At 1 GHz the level of angular broadening produced by this scattering region is roughly 10 times greater than that predicted by a recent model for the distribution of free

electrons in the Galaxy (Taylor & Cordes 1993, hereinafter TC93), even though this model includes a general enhancement of scattering toward the inner Galaxy.

Because all of the sources observed through this region have thus far been Galactic sources, with (presumably) approximately the same location (i.e., in the Galactic center), the radial location of the scattering region is unconstrained. The scattering region could be local to the Galactic center, within approximately 100 pc from the Galactic center—which we refer to as the GC model—or the region could be a random superposition and more than 1 kpc from the GC—which we refer to as the RS model. In the GC model, the region would be a site of excess scattering, and presumably arises from processes unique to the GC; in the RS model, the level of scattering in the region would be high, but not unusually so.

Previous estimates for the location of the scattering region have ranged from 10 pc to 3 kpc. Ozernoi & Shisov (1977) concluded that an “unrealistic” level of turbulence is implied unless the region is within 10 pc of the GC. The level of turbulence they considered unrealistic, however, namely  $\sqrt{\langle n_e^2 \rangle} / \langle n_e \rangle \sim 1$ , does appear to occur elsewhere in the interstellar medium (Spangler 1991). Further, van Langevelde et al. (1992) showed that the free-free absorption toward Sgr A\* would be excessive unless the scattering region was at least 0.85 kpc from the GC, though suitable adjustment of free parameters (outer scale and electron temperature) can decrease the limit to 0.03 kpc. With the free-free absorption they also placed an upper limit on the region’s distance from the GC of 3 kpc. Although the GC model is attractive for phenomenological reasons, other sites of enhanced interstellar scattering are found throughout the Galaxy (e.g., NGC 6634, Moran et al. 1990; Cyg X-3, Molnar et al. 1995) and the mean free path for encountering such a region is approximately 8 kpc (Cordes et al. 1991).

Identifying the location of the scattering region may provide clues to the origin of the scattering. The density fluctuations responsible for interstellar scattering are believed to be generated by velocity or magnetic field fluctuations (Higdon 1984, 1986; Montgomery, Brown, & Matthaeus 1987; Spangler 1991; Sridhar & Goldreich 1994; Goldreich & Sridhar 1995). Velocity or magnetic field fluctuations are also a natural means for inducing anisotropy in the density fluctuations and thereby in the scattering disks. If this supposition is correct, the amplitude of the density fluctuations may provide a measure of the coupling between the density and velocity or magnetic field fluctuations or, more generally, provide information about the small-scale velocity or magnetic field in the scattering region. However, because the radial location of the scattering region is unconstrained, relevant quantities, e.g., the rms density, are uncertain by a factor of  $\Delta_{\text{GC}}/D_{\text{GC}}$ , where  $\Delta_{\text{GC}}$  is the GC-scattering region separation and  $D_{\text{GC}}$  is the GC-Sun distance.

Observations of extragalactic sources viewed through the scattering region could constrain  $\Delta_{\text{GC}}$ ; however, few extragalactic sources have been identified toward the GC. The two sources closest to Sgr A\* are B1739–298 (Dickey et al. 1983) and GPSR 0.539+0.263 (Bartel 1994, private communication), which are 48’ and 40’ from Sgr A\*, respectively. Neither of these is within the region of enhanced scattering defined by the OH masers.

This paper reports VLA and VLBA observations of potential extragalactic sources seen through the GC. Section 2 describes the observations and data reduction, Section 3 discusses the identification of potential extragalactic sources and presents the catalog of sources, Section 4 discusses certain Galactic sources found in our VLA survey, and Section 5 discusses our results and presents our conclusions. A companion paper (Lazio & Cordes 1998, hereinafter Paper II) combines the results of this paper with the previous observations of OH and H<sub>2</sub>O masers and free-free emission in a likelihood analysis that constrains the angular extent and radial location of the scattering region. Paper II also discusses the physical conditions inside the scattering region.

## 2. Observational Program

The scattering diameter of a compact extragalactic source viewed through the scattering region toward the GC is (van Langevelde et al. 1992)

$$\theta_{\text{xgal}} = \frac{D_{\text{GC}}}{\Delta_{\text{GC}}} \theta_{\text{Gal}}, \quad (3)$$

where  $\theta_{\text{Gal}}$  is the characteristic diameter of a GC source. Throughout this paper we will adhere to the convention that scattering diameters are the full width at half maximum of the source’s intensity distribution. We adopt  $D_{\text{GC}} = 8.5$  kpc for the GC-Sun distance (at this distance  $1' = 2.5$  pc), and the observed diameter of Sgr A\* at 1 GHz is  $1''.3$ . Figure 1 shows  $\theta_{\text{xgal}}$  as a function of  $\Delta_{\text{GC}}$ . If the RS model is correct and  $\Delta_{\text{GC}} \gtrsim 1$  kpc, extragalactic source diameters should be a few arcseconds; if the GC model is correct and  $\Delta_{\text{GC}} \approx 100$  pc, source diameters could exceed  $1$  arc min.

Motivated by the prediction illustrated in Figure 1, we undertook a program to identify extragalactic sources toward the GC, measure their angular diameters, and, thus, constrain  $\Delta_{\text{GC}}$ . Scattering diameters of this magnitude are the province of the VLA, and Section 2.1 describes the source selection criteria and the VLA observations in our survey. We also conducted VLBI observations on a subset of the sources detected in our VLA survey; Section 2.2 describes these observations.

### 2.1. VLA Observations

Our initial source list was compiled from previous observations of the GC and contained 15 sources, judged likely to be extragalactic either from spectral information or because the sources appeared compact. The fields observed are listed in Table 1 and are shown in Figure 2; some fields contain more than one source. The fields range in distance from  $7'$  to  $137'$  from Sgr A\*. Such a large range in angular distances from Sgr A\* serves two purposes. First, some of the fields could show heavy scattering, but not at the level seen toward Sgr A\*. These fields will serve as controls. Second, the scattering region could be patchy so that the sources B1739–298 and GPSR 0.539+0.263 are viewed through “holes” in the intense scattering region,

The observations were conducted on 1994 May 15 and 16 in two, eight-hour sessions with the VLA in the BnA configuration. We observed at both 6 and 20 cm. At 20 cm, the array’s resolution is  $5''$  and structure as large as approximately  $1'$  can be detected. It is therefore well-matched to a wide range of scattering diameters, and we hoped to identify extragalactic sources and detect the characteristic  $\lambda^2$  dependence of angular broadening for their angular diameters. For this reason, the AC and BD IFs were centered on 1281 and 1658 MHz, respectively, the widest possible separation allowed by the VLA hardware and radio frequency interference (RFI) environment. We planned to use the 6 cm observations to provide spectral information to assist in the identification of extragalactic sources, and, possibly, to determine intrinsic structure and diameters for sources. The IFs for these observations were centered at 4823 and 4873 MHz. Anticipating the need for a wide field of view to allow for the subtraction of any confusing sources, the observations were conducted in a pseudo-continuum mode. Both right and left circular polarization were recorded in seven, 3-MHz channels; because of edge effects, the total usable bandwidth is 18 MHz per IF. At both bands the resulting bandwidth smearing is negligible even at  $30'$  from the pointing center.

During each eight-hour session, each source was observed at two hour angles for each band. The observations were conducted in snapshot mode, with a duration of 5 min. per hour angle per field. The total observing time per field was 20 min. at 20 cm, obtained over 4 hour angles, and 10 min. at 6 cm, obtained over two hour angles. The resulting theoretical noise level in our images is  $0.4 \text{ mJy beam}^{-1}$  at both bands.

The data were edited and calibrated in the standard fashion within AIPS. The flux scale was set with observations of 3C286 and 3C48; frequent observations of B1748–253 were used to calibrate the visibility phases. For some of the fields at 20 cm, which showed possible gain errors in the dirty images, we also self-calibrated before undertaking the mapping and CLEANing described in §3. Typically one iteration of phase-only self-calibration was applied to the data. The resulting reduction in the off-source rms intensity in images was a factor of 1.5 to 2.

## 2.2. VLBA Observations

As we discuss later, we find a number of compact sources at 20 cm that do not display a  $\lambda^2$  dependence for the angular diameter. Compact sources not showing scattering could arise from several possibilities: First, Galactic sources and extragalactic sources not behind the enhanced scattering region could have diameters much smaller than that of Sgr A\*—the TC93 model predicts a diameter of  $0''.1$  at 1 GHz. Second, if the scattering region is far from Sgr A\*, extragalactic source diameters should be approximately double that of Sgr A\*. That is, source diameters would be  $1''.6$  at 1281 MHz and  $0''.95$  at 1658 MHz. These diameters are sufficiently smaller than the typical beam at 20 cm ( $\approx 5''$ ) that the “deconvolution” of the beam from the measured angular diameters could obscure the effect of scattering, particularly in the presence of noise and at 1658 MHz. Lastly, the scattering screen could be patchy.

In order to test the possibility that the diameters of these compact sources are similar to those predicted by the RS model, we undertook a program of VLBI angular broadening measurements on a small subset of compact sources detected in the VLA program. These sources are listed in Table 2 and are shown in Figure 2.

The sources were observed with a subset of the VLBA—stations PT, LA, KP, FD, OV, and NL—and the phased VLA. Observation wavelengths were 1.3, 3.6, and 6 cm. The wavelengths of observation and VLBI stations were chosen so that the resolution of the array was well-matched to the diameters expected for sources showing broadening typical of the RS model. The resolutions of this array are 1.2 mas at 1.3 cm, 3.9 mas at 3.6 cm, and 6.5 mas at 6 cm; the scattering disk of Sgr A\* is 2 mas at 1.3 cm, 17 mas at 3.6 cm, and 52 mas at 6 cm (Lo et al. 1993; Yusef-Zadeh et al. 1994).

The observations were conducted on 1995 September 22 and 23. Dual polarization was recorded at all three wavelengths, in four 8-MHz IFs, for a total bandwidth of 32 MHz. Data at two hour angles were obtained at 1.3 and 3.6 cm and one hour angle was obtained at 6 cm. However, fringes were not found—even for NRAO 512, an approximately 1 Jy source observed to assist with the fringe finding—during the first hour angle at 1.3 and 3.6 cm. The lack of fringes is due, in part, to receiver problems, as indicated by station logs. The resulting total time on source for all three wavelengths is 5 min., obtained at one hour angle.

The data were analyzed within AIPS. Editing was performed using station-supplied logs; some additional editing, almost exclusively near scan boundaries, was performed later. Amplitude calibration for the VLBA stations was performed using  $T_{\text{sys}}$  measurements for those stations. For baselines including the phased VLA, a source flux density is required. Two of the program sources, B1739–298 and 1LC 359.872+0.178, have fluxes measured over most of the wavelength range of interest (Zoonematkermani et al. 1990; Anantharamaiah & Goss 1994, private communication; §3). The fluxes for the other two program sources were extrapolated from lower frequency measurements assuming the sources had flat spectra. Fluxes for B1741–312 were taken from the VLA calibrator manual (Taylor 1997) and for Sgr A\* from Lo et al. (1993). An opacity correction, based on station-supplied meteorological data, was applied to the 1.3 cm data. Fringe fitting was performed in two steps. First, the delays across individual IFs due to the electronics within the IF were determined. Then the rate, delay between IFs, and the residual delay across individual IFs were determined. Finally, the data were corrected for the shapes (amplitude and phase) of the IF bandpasses at each station. Further analysis on these VLBI data were conducted after integrating them over the full 32 MHz bandpass and for 30 s in time.

### 3. Source Detection, Identification, and Angular Diameter Determination

This section describes the process of source detection in the VLA fields, discusses the extraction of angular diameters from the VLBI observations, and presents the resulting catalogs

and identifications of these sources. Our initial list of candidate extragalactic sources contained 15 targets. Because of the large field of view afforded by the pseudo-continuum observations, we were able to identify well over 100 objects.

### 3.1. Source Detection in the VLA Fields

The intensity distribution of a noise-only image from a multiplying correlator is a gaussian (Fomalont 1988). As Zepka, Cordes, & Wassermann (1994) demonstrated, by comparing the shape of the expected noise-only distribution to that determined from the image itself, it is possible to detect sources below a nominal signal-to-noise threshold. We adapted this source detection procedure in the following manner:

1. Map the primary beam out to the 15 dB level ( $\approx 30'$  at 20 cm and  $\approx 7'$  at 6 cm) and form the intensity histogram of this image;
2. Compare this histogram to a gaussian having the same mean and variance as the image;
3. If the intensity histogram shows deviations, at positive intensities, from a gaussian, locate the deviant pixels in the image, then map and CLEAN a small region around them; and
4. Subtract the CLEAN components of these sources from the visibility data.

This procedure was iterated until the intensity histogram showed good agreement with a gaussian or until deviant pixels could not be identified as sources. Some fields showed symmetrical intensity histograms, though with non-gaussian wings. Such non-gaussian, symmetrical wings can occur because of sidelobes from distant sources or because of RFI.

Our procedure is iterative, in contrast to that described by Zepka et al. (1994) who applied it to X-ray images, because we make use of aperture synthesis images. The beam of an aperture synthesis instrument has high sidelobes (reaching  $\approx 10\%$  of the main beam peak), and the sidelobes extend over the entire image. If not processed in an iterative manner, sidelobes from stronger sources can obscure fainter sources or be identified mistakenly as sources themselves. Isaacman (1981) used a similar iterative procedure in searching for planetary nebulae in the GC, though he used a local signal-to-noise ratio threshold to identify sources.

We call this procedure pdfCLEAN (Lazio & Cordes 1996; Cordes, Lazio, & Sagan 1997): Traditional implementations of CLEAN attempt to reduce an image to the noise level (and then produce a final image by adding CLEAN components to this residual image and smoothing). Moreover, in Clark’s (1980) version of CLEAN, deconvolution of a beam from an image is split into “major” and “minor” cycles. In the major cycle image pixels from which the beam will be deconvolved are identified using a histogram. We view our method of reducing an image histogram

to a noise-only histogram, and in the process identifying image pixels constituting potential sources, as a natural extension of CLEAN methods in general and of Clark’s (1980) method in particular.

The mapping and CLEANing of sources was done independently in each frequency channel. In deciding whether or not deviant pixels constituted a source, we required that sources appear in all six channels and that the CLEANed flux be positive. After mapping and CLEANing a source, a primary beam correction was applied (AIPS task PBCOR) and the intensity was averaged over the channels. At 6 cm the images were also averaged over the two IFs.

We used this procedure on all fields at 6 and 20 cm. For fields within approximately  $1^\circ$  of Sgr A\*, we made minor modifications to the mapping and CLEANing procedure. These fields are distinguished by their intense, extended emission. The emission is sufficiently intense that it is not filtered out completely by the shortest baselines in the BnA configuration, but neither is it sampled sufficiently to be reconstructed accurately by BnA observations alone. We therefore imposed inner  $u$ - $v$  limits, of 1–4 k $\lambda$ , during the mapping. These inner  $u$ - $v$  limits have the effect of reducing further our sensitivity to large angular structures. For the fields with these inner  $u$ - $v$  limits, the largest detectable angular scale is approximately  $30''$ .

For these fields we also knew *a priori* the approximate area over which extended emission would be found (Liszt 1988; Liszt 1994, private communication). The diameters of these regions are arcminutes, in contrast to the typical diameters of the regions we CLEANed in other fields, a few to a few tens of arcseconds. Within these arcminute-sized regions, we therefore accepted as sources only those peaks of emission for which CLEAN components were found in the inner five channels, excluding two channels to allow for edge effects. Many of the sources thus identified appear to be portions of extended emission seen in lower resolution images.

As noted in §2.1, the theoretical noise level in our images is 0.4 mJy beam $^{-1}$ . Through the use of pdfCLEAN we obtained rms noise levels of 0.5–2 mJy beam $^{-1}$  for the various fields, with the fields closest to Sgr A\* having the higher noise levels. In Paper II we shall need the minimum detectable source flux density,  $S_{\min}$ , for each of the survey fields in order to estimate the expected number of extragalactic sources in a field. We determined  $S_{\min}$  from each residual image, i.e., an image formed after subtracting all sources detected in a field. Only the central portion of a residual image, for which the primary beam correction was less than 2%, was used. This region is  $4'$  in size and contains about  $3 \times 10^4$  pixels. The region is large enough that  $1/\sqrt{N}$  is small, but small enough that the primary beam correction is unimportant. We took  $S_{\min} \approx 4\sigma$ ; the minimum flux densities are 2–8 mJy.

The sources detected by our methods are cataloged in Tables 3 (20 cm) and 4 (6 cm). We adopt “1LC” as the catalog designation for the sources we have detected.

If a source has been detected at both 1281 and 1658 MHz, we provide the coordinates from the 1658 MHz identification. Whenever possible we have made gaussian fits, in the image plane (AIPS task JMFIT), to the sources and report the peak and integrated intensity and the “deconvolved” FWHM source diameter. The deconvolution is accomplished by subtracting in quadrature the



beam size ( $\approx 5''$ ) from the fitted diameter. If a gaussian could not be fit to a source, the source was defined to be the polygonal region within which the intensity exceeded  $2\sigma$ ; the peak and integrated intensity within this region are tabulated. The size reported is the product of the number of beams covering the source and the beam size.

For sources detected at both 1281 and 1658 MHz, we report the spectral index ( $S_\nu \propto \nu^{-\alpha}$ ). Some of the sources have extreme spectral indices, with  $|\alpha| > 4$ . We believe that these extreme spectral indices probably reflect a combination of the closely spaced observing frequencies and the primary beam correction rather than the actual spectra. Because the magnitude of the primary beam correction depends upon the distance from the pointing center, we also give this distance.

Table 4 for the sources from the 6 cm survey is similar in format to Table 3 for the sources from the 20 cm survey. We combined the IFs at 6 cm, so we report only one peak intensity, integrated flux, and source diameter measurement. Also, the spectral index is calculated between 6 and 20 cm.

### 3.2. Source Identification

We have compared our sources to the Columbia Galactic plane survey (catalog acronym GPSR) of Zoonematkermani et al. (1990) and Helfand et al. (1992). They surveyed the central Galactic plane,  $-10^\circ \leq \ell \leq 40^\circ$  and  $|b| \leq 1.8^\circ$ , using the VLA, with a similar resolution, at 1.4 GHz. They searched for sources in  $15'$  fields and obtained  $5\sigma$  sensitivities of 5 mJy for fields with  $|b| \approx 1.5^\circ$  to 50 mJy for fields near Sgr A\*. They also compared their catalog to several other surveys and were able to make a number of matches. We classify those sources common to both our survey and the GPSR as Galactic, extragalactic, or unknown. We consider as Galactic those sources having positional coincidences with supernova remnants, planetary nebulae, stars, Einstein X-ray sources, and IRAS sources. A small number of sources are also classified as Galactic by comparison with other surveys of the GC (Yusef-Zadeh & Morris 1987; Liszt 1988). Sources are considered extragalactic if they were identified with galaxies in the GPSR. A small number of sources are also classified as extragalactic by comparison with the VLA calibrator manual (Taylor 1997), the VLBI observations reported here (§3.3), or from other GC VLBI observations (Bartel 1994, private communication).

Figure 3 combines both our survey and the GPSR, indicating whether the sources are Galactic, extragalactic, or as yet unidentified.

Two aspects of the source distribution are evident immediately. First, the fields we have observed have a higher density of sources as compared to those in the GPSR, resulting from both our improved sensitivity and our use of pdfCLEAN. Second, there is a noticeable paucity of sources near Sgr A, and particularly to the northwest.

This paucity could arise from three effects. First, the increase in extended emission near Sgr A will result in an increase in the system temperature and a decrease in the sensitivity. Second, the

majority of the Galactic radio sources found in the GPSR are H II regions (Becker et al. 1992; Helfand et al. 1992). The inner 100 pc or so of the GC are not, on average, a site of current, vigorous star formation, which could contribute to a deficit of Galactic sources (Güsten 1989; Morris & Serabyn 1996). Finally, if the excess scattering region covers this portion of the GC and  $\Delta_{\text{GC}}$  is sufficiently small, extragalactic sources could be broadened to the point that they would be resolved out by both our observations and those of Zoonematkermani et al. (1990). To evaluate these possibilities quantitatively, we performed a likelihood analysis that is described in Paper II, where we find that this paucity is due, in part, to hyperstrong scattering occurring in the GC.

### 3.3. Angular Diameters from VLBI Measurements

For the bandwidth (32 MHz) and integration time (30 s) used, the expected rms visibility in the total intensity for a VLBA-VLBA baseline is approximately 10 mJy at 6 cm, 15 mJy at 3.6 cm, and 50 mJy at 1 cm; the VLBA-VLA baselines should have an rms a factor of  $\sqrt{27}$  smaller than that of the VLBA-VLBA baselines. We also considered an integration time of 60 s in an effort to detect sources or improve the signal-to-noise ratio for weak sources. Longer integration times, though allowed by the coherence time at 3.6 and 6 cm, produced few visibilities on any given baseline and were not used.

If the signal-to-noise ratio in the visibility data for a source is sufficiently high, we have fit a circular gaussian. Our limited hour angle coverage does not justify more complicated models. For those sources showing marginal detections, we attempted to assess their structure using the rms visibility phase,  $\sigma_\phi$ . Thompson, Moran, & Swenson (1986) show that, in the low signal-to-noise case, the visibility modulus is

$$\frac{|V|}{\sigma} \approx \frac{\pi\sqrt{2}}{3} \left( 1 - \frac{\sqrt{3}}{\pi}\sigma_\phi \right), \quad (4)$$

where  $\sigma^2$  is the variance of the visibility modulus. If  $|V|/\sigma \rightarrow 0$ , the distribution of the visibility phase is uniform on the interval 0 to  $2\pi$ . For weak sources we have compared the visibility phases to a uniform distribution using the Kolmogorov-Smirnov statistic. For those baselines for which the phases are not consistent with a uniform distribution, we compute  $|V|/\sigma$  using equation (4).

We discuss the results for each source separately.

#### 3.3.1. *Sgr A\**

We observed *Sgr A\** primarily as a control source. It is detected at all three frequencies. The source diameters we derive are consistent with those expected from previous measurements (viz. §2.2):  $51.6 \pm 0.8$  mas at 6 cm,  $16.6 \pm 0.4$  mas at 3.6 cm, and  $2.3 \pm 0.2$  mas at 1.3 cm.

### 3.3.2. B1741–312 (1LC 357.862–0.997)

This source is a VLA calibrator source (Taylor 1997) and is described by Backer (1988) as “heavily scattered.” We detect it at all three frequencies. While not as heavily scattered as Sgr A\* (its scattering diameter is a factor of 5 smaller), its 1 GHz scattering diameter is approximately a factor of 2 larger than that predicted by the TC93 model. Its diameters are  $18.2 \pm 0.4$  mas at 6 cm,  $7.2 \pm 0.2$  mas at 3.6 cm, and  $1.0 \pm 0.1$  mas at 1.3 cm; these diameters scale as  $\lambda^{1.8 \pm 0.4}$ .

### 3.3.3. B1739–298 (1LC 358.918+0.073)

This source is located approximately  $1^\circ$  from Sgr A\*. Most of its displacement from Sgr A\* is in longitude and it provides a constraint on the extent of the screen to negative longitudes.

At 6 cm this source is detected clearly on short baselines, Figure 4, and it has a diameter of  $27.9 \pm 1.9$  mas. At 3.6 cm this source is only marginally detected on the inner baselines which include the phased VLA; we can place only an upper limit of 55 mas on its diameter. At 1 cm this source is not detected. This non-detection is consistent with the source’s spectrum: At 3.6 cm the source has a flux of approximately 30 mJy (Zoonematkermani et al. 1990) and between 6 and 3.6 cm, its spectral index is 1.9 ( $S \propto \nu^{-\alpha}$ ). At 1.3 cm, its expected flux is therefore approximately 5 mJy, well below our detection threshold.

We have attempted to determine an angular diameter for the source at 18 cm from our VLA observations. From a super-uniformly-weighted image we find a diameter of  $0''.86$ . This diameter is likely to be an upper limit. Taking  $\theta \propto \lambda^\beta$  between 6 and 18 cm,  $\beta = 3$ , far steeper than predicted even by scattering.

The source’s 6 cm diameter is larger than predicted by the TC93 model (a factor of 5), but smaller than that of Sgr A\* (a factor of 2). Scaling its 6 cm diameter to 18 cm, assuming a  $\lambda^2$  dependence for the angular diameter, its predicted scattering disk at 18 cm is 250 mas. This diameter is comparable to many of the OH masers with  $\ell < 0^\circ$  and  $|b| \gtrsim 1.5^\circ$  (van Langevelde et al. 1992), yet  $b = 0.07^\circ$  for B1739–298. In both the GC and RS models presented in §1, extragalactic sources seen through the enhanced scattering region must have diameters larger than that of Sgr A\*, viz. Figure 1. Galactic sources can have a range of source diameters, depending upon whether they are behind the scattering region or not and, if behind the scattering region, their distance from the region.

This source is extragalactic: A lower limit to its brightness temperature is  $10^6$  K and it is detected in the Texas survey at 365 MHz (Douglas et al. 1996). The H I absorption towards this source places a lower limit of 25 kpc on its distance (Dickey et al. 1983). The H I spectra of this source and the VLA calibrator B1741–312 are similar in shape and cover nearly the same velocity range ( $-80$  km s $^{-1}$  to  $50$  km s $^{-1}$ , with B1739–298 showing additional weak emission to  $100$  km s $^{-1}$ ). Further, compact Galactic sources are typically also X-ray sources, e.g., Cyg X-1 and

the central component of 1E 1740.7–2947; there are no X-ray sources within  $5'$  of this source.

Because this source is extragalactic and its diameter is smaller than that of Sgr A\*, we cannot use it to constrain the radial location of the screen. However, in conjunction with the heavily scattered maser OH 359.517+0.001, we shall use it to constrain the angular extent of the scattering region to negative longitudes to be less than  $1^\circ$  (Paper II).

### 3.3.4. 1LC 358.439–0.211

We do not detect this source at any of the three frequencies. The source’s 6 cm flux is 38 mJy (Becker et al. 1994); there are no higher frequency observations of this source. At 6 cm this source should be a  $3\text{--}4\sigma$  detection on VLBA-VLBA baselines. Several possibilities exist for the source’s non-detection:

**Resolved out:** Table 2 lists the angular diameter the source would need to have in order to be resolved out by the shortest baseline, PT-VLA. Becker et al. (1994) determine a diameter of  $2''.2$  from a naturally-weighted image; we did not observe this source in our 6 cm observations. The actual 6 cm diameter could be much smaller because, in a super-uniformly-weighted image from our 1658 MHz VLA observations, the source has a diameter of  $1''$ , only slightly larger than the diameter of B1739–298.

**Structure:** Complex structure produces nulls in the visibility plane. For example, a double source produces a cosinusoidal visibility function (Pearson 1995). If this source is a double with a separation of 200–250 mas, the correlated flux at 6 cm on the innermost baselines would be reduced substantially below the nominal 38 mJy.

**Spectrum:** The source has a spectrum  $S \propto \nu^{-0.3}$  between 1.4 and 5 GHz. If we extrapolate this spectrum to 1.3 cm, the expected flux is 25 mJy, which would be detectable on only the VLBA-VLA baselines. The expected 3.6 cm flux is 33 mJy, which would be marginally detectable on VLBA-VLBA baselines (via eqn. [4]). If the spectrum steepens at higher frequencies, these flux densities would be correspondingly reduced.

**Variability:** There has been only one 6 cm observation of this source and two measurements at 20 cm of its flux. The two measurements at 20 cm (the GPSR and ours) agree to better than 5% and are separated by 5 yr.

**Position Error:** Position errors lead to fringe rates and delays. If the rate and delay windows are too small during the fringe fitting, fringes will not be found. The position for the source was obtained from our VLA observations and is accurate to approximately  $1''$ . The rate and delay windows we used allow position errors of several arcseconds.

Of these possible causes, we favor the spectrum as the reason for the non-detection at 1.3 cm and source structure for its non-detection at 3.6 and 6 cm.

### 3.3.5. *1LC 359.872+0.178*

Located approximately  $15'$  from Sgr A\*, displaced largely in latitude, detection of scattering from this source would place severe constraints on the angular extent of the screen, and possibly on the radial distance as well. Section 4 summarizes a number of measurements of this source; here the focus is on just the VLBI measurements.

We do not detect this source at any of the three frequencies. Based on the flux measurements summarized in §4, the lack of detection at 1 cm is consistent with the source’s spectrum. At 3.6 cm the flux density is comparable to the expected rms visibility, and, at best, only a marginal detection using the visibility phases could be obtained (eqn. 4). At 6 cm our attempts to detect this source have included both global and baseline-based approaches to fringe fitting, and, in the global fringe fitting, utilizing different rate and delay windows and different solution intervals.

The lack of a detection at 6 cm is most likely due to source being sufficiently extended as to be resolved out. The shortest baselines in our VLBI array are those on the LA-PT-VLA triangle which are sensitive to angular structure on a scale of approximately  $0''.2$ . This source is a double, with a component separation of  $4''$ . The stronger component, the one observed, has a flux of 20 mJy at 6 cm. Yusef-Zadeh, Cotton, & Reynolds (1998) have presented higher resolution VLA observations of this source at 2 and 6 cm. At 6 cm they find the stronger component to have a diameter of approximately  $0''.4$ . Subsequent to the VLA observations we present here, we obtained slightly higher resolution observations at 6 cm; we find a diameter similar to that found by Yusef-Zadeh et al. (1998). Further, they show that at 2 cm, the structure of the stronger component is resolved into two slightly extended subcomponents with a “barrel-shaped appearance.” The other component is unresolved (Yusef-Zadeh et al. 1998), but is sufficiently weak ( $\approx 5$  mJy) that we would not have been able to detect it.

### 3.3.6. *1LC 0.846+1.173*

This source is not detected at any of the three frequencies. As for 1LC 358.439–0.211, we quote the angular diameter the source would need in order to be resolved out.

Of the causes listed for the non-detection of 1LC 358.439–0.211, the spectrum is the most likely cause for this source’s non-detection at 1.3 and 3.6 cm with source structure the cause at 6 cm. There is no measurement of this source’s flux above 1.4 GHz: It was sufficiently far from the center of the closest field at 6 cm that we have no observations of it and it was outside the Galactic latitude limit of the survey by Becker et al. (1994). It is detected in the Texas survey (Douglas et al. 1996) and has a 0.3–1.4 GHz spectral index of 0.9. At 6 cm we expect a flux of 50 mJy, comparable to B1739–298. Variability is an unlikely cause as the two flux determinations at 20 cm (the GPSR and ours) agree to better than 5%.

We observed this source, even though it has a steep spectrum, because it is at fairly high

latitude. Most of our fields and most of the OH/IR stars with measured angular diameters are distributed in longitude, so that there are few constraints on the latitude distribution of scattering. A measured angular diameter could have improved our knowledge of the latitude distribution of scattering. As it happens, this source is drawn from a field in which the number of sources is consistent with that expected from extragalactic source counts (Paper II), implying that scattering is unlikely to dominate this source’s angular diameter and that it is unlikely to be resolved out.

#### 4. Galactic Sources from the Survey

Our primary aim in this project was to identify extragalactic sources suitable for angular broadening measurements. In the course of our survey, we found a number of Galactic sources, a subset of which is described here.

##### 4.1. 1LC 359.872+0.178

The source 1LC 359.872+0.178 (source 35W44, Isaacman 1981; source J, Yusef-Zadeh & Morris 1987; GPSR 359.873+0.179, Zoonematkermani et al. 1990) is located approximately  $15'$  from Sgr A\* and potentially within the region of enhanced scattering detected by van Langevelde et al. (1992) and Frail et al. (1994). At high frequencies it has two components, suggestive of an extragalactic source. If it is extragalactic, it sets important constraints on the scattering region in front of Sgr A\*. Namely, it implies either that the RS model is correct, or that, if the GC model is correct, the scattering region is patchy or does not extend to more than  $15'$  in latitude. Alternately, the source could be Galactic, in which case it could be an X-ray-quiet version of 1E 1740.7–2942 (Mirabel et al. 1992). Yusef-Zadeh et al. (1998) argue that the two components are unrelated—based on their slightly different spectral indices, and that the stronger of the two is a candidate young supernova remnant.

This section summarizes observations of this source at a variety of wavelengths. We conclude that if it is scattered, the source is Galactic. The source’s spectrum and apparent diameter are shown in Figure 5; its spectral index ( $S \propto \nu^{-\alpha}$ ) over the observed frequency range is  $\alpha \approx 1$ . The spectrum shown in Figure 5 is constructed from observations with considerably different resolutions over a time span of approximately 10 yrs. Thus, it should be taken as indicative of the actual spectrum, though a spectrum found from observations with matched resolutions might not be quite as steep.

#### 4.1.1. *Summary of Observations*

In addition to the observations summarized here, we have obtained additional observations of this source at 6 and 20 cm (and 90 cm) with the VLA with slightly higher resolutions than those described here. These observations are in the process of being reduced and the results will be presented elsewhere (Lazio et al. 1998). However, preliminary indications are that source structure and diameters from these observations are consistent with those reported here.

**1.3cm** In this paper we report a non-detection of this source in a VLBI experiment. This non-detection is consistent with the source’s spectrum extrapolated from longer wavelengths. Our sensitivity was 50 mJy, and the source’s flux is expected to be approximately 10 mJy.

**2cm** Yusef-Zadeh et al. (1998) present a VLA image with a resolution of  $0''.36 \times 0''.13$ . The source is a double with separation of approximately  $4''$ . The northern component, component A, is the brighter of the two and has a complex structure, approximately  $0''.5$  in diameter with a “barrel-shaped appearance.” The southern component, component B, is possibly resolved into a compact core and a weak halo.

Anantharamaiah & Goss (1994, private communication) imaged the source with the VLA, though with a resolution of only  $2''.6 \times 1''.2$ . Component A appears unresolved and has a flux of 9.9 mJy. Component B is slightly resolved and has a flux of approximately 2 mJy.

**3.5cm** Anantharamaiah & Goss (1994, private communication) also obtained VLA observations at 3.5 cm contemporaneously with the 2 cm observations. At their resolution of  $4''.6 \times 2''.7$ , the source is a partially resolved double, again with a separation of approximately  $4''$ . Component A is again unresolved and has a flux of approximately 20 mJy. Component B is, at best, mildly resolved and has a flux of approximately 4 mJy. There is a faint source visible, with a flux density of approximately 1 mJy and located approximately  $7''$  to the southeast, which may be a third component of this source.

We were unable to detect this source in a VLBI experiment. However, the expected rms visibility for our VLBA-VLBA baselines is 15 mJy, so a detection on these baselines would be only marginal. On the VLBA-VLA baselines, the rms visibility is 3 mJy, so we would have expected this source to be approximately a  $5\sigma$  detection. As we discuss in §3.3.5, we attribute this non-detection to be the result of source structure.

**6cm** Yusef-Zadeh et al. (1998) present both total and polarized intensity images obtained with the VLA with a resolution of  $0''.98 \times 0''.34$ . In total intensity, the source can still be identified as a double, but only component A is present in the polarized image. Component A has a diameter of

approximately  $0''.5$  while component B is unresolved. The total integrated flux is 28 mJy and the polarized flux is 2.4 mJy (Yusef-Zadeh 1994, private communication).

Becker et al. (1994) detect this source in their 6 cm survey of the Galactic plane. They find a flux of 37.2 mJy. From a naturally-weighted image with a resolution of approximately  $4''$ , they fit a single gaussian to obtain a source diameter of  $1''.3$ .

We observed this source as part of our VLA program. We find it to be a nearly resolved double with a separation of  $3''.7$ . The integrated flux is 41.9 mJy. Fitting two gaussians to a naturally-weighted image, we find the northern component to have a diameter  $0''.71 \times 0''.47$ . Our subsequent, slightly higher resolution observations indicate that component A’s diameter is approximately  $0''.4$ .

We did not detect this source in a VLBI experiment. The expected rms visibility for our VLBA-VLBA baselines is 10 mJy, so that on these baselines we would expect a  $3\sigma$  detection, and a  $15\sigma$  detection on VLBA-VLA baselines. The higher frequency observations described above indicate that the probable cause for the non-detection is source structure.

**18–21cm** At 1400 MHz the source has a flux of 267 mJy. When fit with a single gaussian, the source has a diameter of  $3''.8$ ; the resolution of these observations was approximately  $5''$  (Zoonematkermani et al. 1990). However, the source was  $20''.7$  from the phase center of their observation, so the flux density measurement has a relatively large uncertainty because of the large primary beam correction.

Anantharamaiah & Goss (1994, private communication) also imaged the source at 1477 MHz, though not contemporaneously with the observations described above. With a resolution of approximately  $5''$ , the source is unresolved and has an integrated flux of 154 mJy.

We have observations of this source at 1281 and 1658 MHz from our VLA program. At 1281 MHz, the integrated flux is 66.9 mJy and, at 1658 MHz, it is 83.1 mJy. These are likely to be lower limits to the actual values as inner  $u$ - $v$  cutoffs of 1–4  $k\lambda$  were used in the imaging. Super uniformly-weighted images at both 1281 and 1658 MHz, with resolutions of approximately  $3''.2 \times 2''.6$ , show the source to be unresolved.

**35cm** Gray (1996, private communication) detected this source in the 843 MHz MOST survey (Gray 1994). The flux density of the source is 480 mJy. The beam diameter of the MOST is too large,  $90'' \times 45''$ , to derive a reliable angular diameter.

**90cm** Anantharamaiah et al. (1991) used the the VLA to observe the GC. The VLA’s primary beam at 90 cm is large enough that this source was included in the field of view. They find a flux of 580 mJy for the source. The diameter is  $19''.8 \times 18''.6$  at  $170^\circ$  (Anantharamaiah & Goss 1994, private communication). The beam is approximately  $11''$ . Based on their (brief) description, this source is probably only mildly resolved, with a “deconvolved” diameter of  $16''$ .



**375cm** The line of sight toward the source shows strong absorption and the source cannot be identified (LaRosa & Kassim 1985).

#### 4.1.2. Scattering

The source is  $15'$  from Sgr A\*, with most of the displacement in Galactic latitude, and is potentially seen through the scattering region responsible for the enhanced broadening of Sgr A\* and the OH/IR stars (in particular, see Fig. 2 of Frail et al. 1994). The actual amount of broadening expected for this source depends upon its distance from the Sun and the Galactic center-scattering screen distance,  $\Delta_{\text{GC}}$ . Throughout we focus on component A as it is stronger, and more complete information exists for it. The diameters summarized above are shown in Figure 5.

We first determine if scattering dominates the observed angular diameters. We solve for the source’s diameter dependence with wavelength,  $\theta \propto \lambda^\beta$ . If scattering determines the observed diameter, we would expect  $\beta = 2$ . Using the measured diameters at 0.3 and 1.4 GHz, where scattering is most likely to dominate,  $\beta \approx 1.3$ . If we use this angular dependence to predict the diameter at 6 cm, we find an angular diameter  $\theta \approx 0''.4$ , comparable to that which is observed. However, this estimate does not allow for the intrinsic source structure indicated by the higher frequency observations.

In order to allow for intrinsic source structure, we model the apparent source diameter,  $\theta_{\text{app}}$ , as a function of frequency

$$[\theta_{\text{app}}(\nu)]^2 = \left( \frac{\theta_s}{\nu_{\text{GHz}}^2} \right)^2 + \theta_i^2 \quad (5)$$

with  $\nu_{\text{GHz}}$  the observation frequency in GHz,  $\theta_s$  the scattering angle at the nominal frequency of 1 GHz, and  $\theta_i$  the intrinsic diameter, i.e., the diameter the source would have in the absence of any scattering, at 1 GHz. Motivated by the complex structure seen at 2 cm (Yusef-Zadeh et al. 1998), we have assumed that the intrinsic source diameter is relatively frequency independent. Any intrinsic source structure whose frequency dependence is of the form  $\nu^\gamma$  with  $\gamma < 0$  will only strengthen our conclusions. From the higher frequency observations described above, we take  $\theta_i = 0''.4$ , the diameter of the stronger component, component A.

If the source is Galactic and the source is behind the scattering screen,  $\theta_s = 1''.3$ , namely the diameter of Sgr A\*. In this case we expect  $\theta_{\text{app}} = 0''.77$  at 1.4 GHz and  $\theta_{\text{app}} = 12''$  at 0.33 GHz. This predicted 1.4 GHz diameter is similar to that observed for Sgr A\*. More importantly, the highest resolution observations at 1.4 GHz have a resolution of  $2''.9$ . The beam is sufficiently larger than the predicted diameter of the source that we expect the source to be unresolved, as is indeed found. The observed diameter at 0.33 GHz is 25% larger than this value. A larger diameter could be obtained if the source-screen separation is slightly larger than that of the Sgr A\*-screen separation. Cordes & Lazio (1997) show that a source a distance  $\Delta$  behind the scattering screen has a scattering diameter of  $\theta_s \simeq \theta_{\text{Gal}}(\Delta/\Delta_{\text{GC}})$ . If the Sgr A\*-scattering region separation is  $\Delta_{\text{GC}} = 150$  pc (Paper II), then

a source-scattering region separation of  $\Delta = 190$  pc, i.e., the source would be 40 pc more distant than Sgr A\*, would be sufficient to explain the observed diameter at 0.33 GHz.

The scattering toward the GC is so intense that our analysis of the 0.33 GHz diameter does not depend upon what we assume for the intrinsic diameter of the source. Since the scattering diameter determines the minimum diameter of the source in strong scattering (Cohen & Cronyn 1974), we could have taken the intrinsic diameter to be the  $4''$  separation of the two components. If we had done so, our prediction for the apparent diameter at 0.33 GHz would have increased to only  $\theta_{\text{app}} = 12''.5$ , and our conclusions would not have been affected.

If the source is extragalactic *and* behind the Sgr A\* scattering screen, then, from equation (3), the minimum value of  $\theta_s$  is approximately double the diameter of Sgr A\* or  $2''.6$ , which occurs when the scattering region is midway between the Sun and the GC. Even this minimal value of scattering for an extragalactic source is too much, however. In this case, the predicted apparent diameter at 0.33 GHz is  $\theta_{\text{app}} = 24''$ , 50% larger than the diameter of  $16''$ .

We conclude that this source is unlikely to be extragalactic *and* affected by the scattering screen in front of Sgr A\*. Its morphology is suggestive of an extragalactic source, in which case it would indicate that the extent of the scattering screen to positive latitudes is no more than  $15'$  (implying an axial ratio for the scattering screen of at least 0.6) or that the scattering material is patchy. Alternately, the source could be Galactic, in which case it is likely to be no more than approximately 40 pc more distant than Sgr A\*.

#### 4.2. 1LC 358.600–0.060

This source is within the star-formation region Sgr E and appears to be a central point source surrounded by a shell, Figure 6. Previous observations at 1.4 GHz could not resolve the point source (Gray et al. 1993).

On the basis of a nearly flat spectral index, Gray et al. (1993) conclude that this source is an H II region. They determine a shell diameter of nearly  $100''$ , and their image shows considerable diffuse emission in the region of this source. Our image of the shell-like structure shows a more limited extent. We have formed a spectral-index map from our images at 1281 and 1658 MHz. Much, but not all, of the shell is marked by a steep spectral index,  $\alpha \gtrsim 1$ . The central point source also appears to have a steep spectral index, though it is not distinguished clearly from the rest of the structure.

From the morphology and spectral information, we classify this object tentatively as a supernova remnant. Polarization information would be useful in making a final determination.

### 4.3. GPSR 358.960+0.555

This object is a compact, 8–10 mJy source found by Zoonematkermani et al. (1990). The source is located  $4'$  from the phase center of their field 359.0+0.5, so that the primary beam correction is not large. This position is  $2'$  from the phase center of our field 358.9+0.5. Within a  $30''$  radius of the quoted position for this source, we find no source brighter than  $1.5 \text{ mJy beam}^{-1}$ .

Zoonematkermani et al.’s (1990) minimum detectable flux for this field is 10 mJy. This source is either a misidentified noise fluctuation or another Galactic radio transient (Davies et al. 1976; Zhao et al. 1992).

## 5. Conclusions

This paper has reported the results of a program to identify and obtain scattering diameters for extragalactic sources seen through the Galactic center scattering region. Because they are located far behind the GC, the scattering diameters of extragalactic sources, when compared to the scattering diameter of GC sources such as Sgr A\*, can constrain the *radial* location of the scattering region, viz. equation (3) and Figure 1.

Using the VLA we observed 10 (11) fields at 20 cm (6 cm) containing 15 suspected extragalactic sources. We increased our catalog of sources to well over 100 through the use of pdfCLEAN: The intensity histogram of the primary beam was used to identify positive brightness image pixels that produced deviations from the shape of the expected noise-only histogram. We found approximately 10 sources per field.

Follow-up VLBI observations on a subset of these sources have determined the scattering diameters for two heavily scattered extragalactic sources. Their diameters are too small, by factors of 4–10, for them to be seen through the scattering region in front of Sgr A\*. However, they can be used, in conjunction with the heavily scattered masers, to set constraints on the angular extent of the region.

Our fields show a paucity of sources near Sgr A\*; a previous survey with more uniform sky coverage, but at a lower sensitivity also shows a paucity. Such a deficit could arise if the scattering toward the GC is so severe that our (and previous) observations resolve out extragalactic sources. The sources reported here are combined with angular broadening measurements of Sgr A\* and OH masers and free-free emission and absorption measurements from the literature. These data are then used in a likelihood analysis to determine the model parameters of the GC scattering region (Paper II).

We thank M. Goss and F. Yusef-Zadeh for contributing information on 1LC 359.872+0.178. We thank the many GC observers who contributed potential extragalactic sources during the early stages of this project. We thank N. Bartel for contributing additional angular broadening

measurements. H. Liszt contributed data prior to publication. The Very Large Array (VLA) and the Very Long Baseline Array (VLBA) are facilities of the National Science Foundation operated under cooperative agreement by Associated Universities, Inc. This research made use of the Simbad database, operated at the CDS, Strasbourg, France. This research was supported by the NSF under grant AST 92-18075 and AST 95-28394. The NAIC is operated by Cornell University under a cooperative agreement with the NSF. TJWL holds a National Research Council-NRL Research Associateship. Basic research in astronomy at the Naval Research Laboratory is supported by the Office of Naval Research.

## REFERENCES

- Anantharamaiah, K. R., Pedlar, A., Ekers, R. D., & Goss, W. M. 1991, *MNRAS*, 249, 262
- Backer, D. C., Zensus, J. A., Kellermann, K. I., Reid, M., Moran, J. M., & Lo, K. Y. 1993, *Science*, 262, 1414
- Backer, D. C. 1988, in *Radio Wave Scattering in the Interstellar Medium*, eds. J. M. Cordes, B. J. Rickett, & D. C. Backer (New York: AIP) p. 111
- Becker, R. H., White, R. L., Helfand, D. J., & Zoonematkermani, S. 1994, *ApJS*, 91, 347
- Becker, R. H., White, R. L., McLean, B. J., Helfand, D. J., & Zoonematkermani, S. 1992, *ApJ*, 358, 485
- Clark, B. G. 1980, *A&A*, 89, 377
- Cohen, M. H. & Cronyn, W. M. 1974, *ApJ*, 192, 195
- Condon, J. J., Broderick, J. J., & Seielstad, G. A. 1991, *AJ*, 102, 2041
- Cordes, J. M., Lazio, T. J. W., & Sagan, C. 1997, *ApJ*, 487, 782
- Cordes, J. M., Weisberg, J. M., Frail, D. A., Spangler, S. R., & Ryan, M. 1991, *Nature*, 354, 121
- Davies, R. D., Walsh, D., & Booth, R. S. 1976, *MNRAS*, 177, 319
- Davies, R. D., Walsh, D., Browne, I. W. A., Edwards, M. R., & Noble, R. G. 1976b, *Nature*, 261, 476
- Dickey, J. M., Kulkarni, S. R., van Gorkom, J. H., & Heiles, C. 1983, *ApJS*, 53, 591
- Douglas, J. N., Bash, F. N., Bozayan, F. A., Torrence, G. W., & Wolfe, C. 1996, *ApJ*, 111, 1945
- Fomalont, E. B. 1988, in *Synthesis Imaging in Radio Astronomy*, eds. R. A. Perley, F. R. Schwab, & A. H. Bridle (ASP: San Francisco) p. 231
- Frail, D. A., Diamond, P. J., Cordes, J. M., & van Langevelde, H. J. 1994, *ApJ*, 427, L43
- Goldreich, P. & Sridhar, S. 1995, *ApJ*, 438, 763
- Gray A. D. 1994, *MNRAS*, 270, 822
- Gray A. D., Whiteoak J. B. Z., Cram L. E., & Goss W. M. 1993, *MNRAS*, 264, 678
- Güsten, R. 1989, in *The Center of the Galaxy*, ed. M. Morris (Dordrecht: Kluwer) p. 89
- Helfand, D. J., Zoonematkermani, S., Becker, R. H., & White, R. L. 1992, *ApJS*, 80, 211
- Higdon, 1986, *ApJ*, 309, 342

- Higdon, 1984, *ApJ*, 285, 109
- Isaacman, R. 1981, *A&AS*, 43, 405
- Ishimaru, A. 1978, *Wave Propagation and Scattering in Random Media* (San Diego: Academic)
- Krichbaum, T. P. et al. 1993, *A&A*, 274, L37
- Larosa, T. N. & Kassim, N. E. 1985, *ApJ*, 299, L13
- Lazio, T. J. W., Cordes, J. M., Kassim, N. E., & Arzoumanian, Z. 1998, in preparation
- Lazio, T. J. W. & Cordes, J. M. 1998, *ApJ*, in press (Paper II)
- Lazio, T. J. W. & Cordes, J. M. 1996, in *The Galactic Center*, ed. R. Gredel (San Francisco: ASP) p. 127
- Liszt, H. 1988, in *Galactic and Extragalactic Radio Astronomy*, eds. G. L. Vershuur & K. I. Kellermann (Berlin: Springer-Verlag) p. 359
- Lo, K. Y., Backer, D. C., Kellermann, K. I., Reid, M., Zhao, J. H., Goss, W. M., & Moran, J. M. 1993, *Nature*, 362, 38
- Mirabel, I. F., Rodríguez, L. F., Cordier, B., Paul, J., & Lebrun, F. 1992, *Nature*, 358, 215
- Molnar, L. A., Mutel, R. L., Reid, M. J., Johnston, K. J., 1995, *ApJ*, 438, 708
- Montgomery, D., Brown, M. R., & Matthaeus, W. H. 1987, *J. Geophys. Res.*, 92, 282
- Moran, J. M., Rodríguez, L. F., Greene, B., Backer, D. C. 1990, *ApJ*, 348, 150
- Morris, M. & Serabyn, E. 1996, *ARA&A*, 34, 645
- Ozernoi, L. M. & Shishov, V. I. 1977, *Pis'ma Astron. Zh.*, 3, 435 (*Sov. Astron. Lett.*, 3, 233)
- Pearson, T. J. 1995, in *Very Long Baseline Interferometry and the VLBA*, eds. J. A. Zensus, P. J. Diamond, & P. J. Napier (San Francisco: ASP) p. 267
- Rogers, A. E. E. et al. 1994, *ApJ*, 434, L59
- Spangler, S. R. 1991, *ApJ*, 376, 540
- Sridhar, S. & Goldreich, P. 1994, *ApJ*, 432, 612
- Taylor, G. 1997, [URL:http://www.nrao.edu/%7Eegtaylor/calib.html](http://www.nrao.edu/%7Eegtaylor/calib.html)
- Taylor, J. H. & Cordes, J. M. 1993, *ApJ*, 411, 674 (TC93)
- Thompson, A. R., Moran, J. M., & Swenson, G. W., Jr. 1986, *Interferometry and Synthesis in Radio Astronomy* (New York: Wiley)

- van Langevelde, H. J., Frail, D. A., Cordes, J. M., & Diamond, P. J. 1992, *ApJ*, 396, 686
- Yusef-Zadeh, F., Cotton, W. D., & Reynolds, S. P. 1998, *ApJ*, submitted
- Yusef-Zadeh, F., Cotton, W., Wardle, M., Melia, F., & Roberts, D. A. 1994, *ApJ*, 434, L63
- Yusef-Zadeh, F. & Morris, M. 1987, *ApJ*, 320, 545
- Zepka, A. F., Cordes, J. M., & Wassermann, I. 1994, *ApJ*, 427, 438
- Zhao, J., et al. 1992, *Science*, 255, 1538
- Zoonematkermani, S., Helfand, D. J., Becker, R. H., White, R. L., & Perley, R. A. 1990, *ApJS*, 74, 181

Fig. 1.— The diameter of an extragalactic source at 1.4 GHz seen through the scattering region in front of Sgr A\* as a function of the Galactic center-scattering region distance,  $\Delta_{GC}$ . The dotted line indicates an extreme lower limit on  $\Delta_{GC}$  as derived from the lack of free-free absorption toward Sgr A\* at centimeter wavelengths. At this frequency, the scattering diameter of Sgr A\* is  $0''.7$ . The scattering diameter scales as  $\theta_s \propto \nu^{-2}$ .

Fig. 2.— Fields observed with the VLA and sources observed with the VLBA. Large, solid circles show the half-power primary VLA beam width at 1658 MHz. Small, dashed circles show the half-power primary beam at 4863 MHz. Crosses are the VLBI program sources and asterisks are the control sources Sgr A\* and B1741–312. The contours are from the 5 GHz survey with the NRAO 91 m telescope (Condon, Broderick, & Seielstad 1991) and are at 0.32, 0.64, 1.28, 2.56, 5.12, 10.2, 20.5, 41, and 82% of the peak, 250 Jy beam<sup>-1</sup>. Breaks in the contours result from gaps in the original survey.

Fig. 3.— Radio sources detected in this work and by Zoonematkermani et al. (1990) and Helfand et al. (1992). Sources are represented by *asterisks* if they are Galactic, *circles* if extragalactic, and by *triangles* if unidentified. See text for criteria for distinguishing Galactic from extragalactic sources. The large circles are the fields observed at 20 cm, cf. Figure 2.

Fig. 4.— Correlated flux density as a function of projected baseline for B1739–298 at 6 cm. The solid line shows a circular gaussian with a diameter of 27.9 mas.

Fig. 5.— 1LC 359.872+0.178. (a) The spectrum of the northern component. (b) The apparent diameter of the northern component. The dashed line shows the angular diameter dependence if angular broadening dominates the source size.

Fig. 6.— 1LC 358.600–0.060, a shell-like source with an embedded point source detected in our survey. (Top) Total intensity. Contours are in units of  $0.96 \text{ mJy beam}^{-1} \times -2, 2, 3, 5, 7.07, 10, \dots$ , the size of the beam is shown in the lower left. (Bottom) Spectral index between 1281 and 1658 MHz. Contours are  $-1.5, -1.0, -0.5, 0.5, 1.0$ , and  $1.5$ ; negative contours are dashed.



Table 1. Pointing Centers

Field	RA (J2000)	Dec (J2000)	Sgr A* Distance (')
357.9–1.0	17 44 23.5	–31 16 35	137
358.1–0.0 <sup>b</sup>	17 41 17.0	–30 33 00	113
358.2–0.0 <sup>a</sup>	17 41 23.0	–30 30 02	110
358.7–0.0	17 42 34.0	–30 05 38	80
358.9+0.5	17 40 54.0	–29 29 49	77
359.9+0.2	17 44 36.0	–28 57 10	16
0.0+0.0 <sup>a</sup>	17 45 30.0	–28 54 39	6
0.0+0.0 <sup>b</sup>	17 45 36.0	–28 53 20	7
0.2–0.7	17 48 48.0	–29 07 38	47
0.5+0.2	17 45 52.0	–28 20 25	40

Table 1—Continued

Field	RA (J2000)	Dec (J2000)	Sgr A* Distance (')
1.0+1.6	17 42 03.0	−27 13 23	120
1.1−0.1 <sup>a</sup>	17 48 33.0	−28 02 30	72
1.2−0.0 <sup>b</sup>	17 48 31.0	−27 55 00	78
1.3−0.0 <sup>a</sup>	17 48 51.0	−27 51 55	84
3.7+0.6 <sup>c</sup>	17 51 51.2	−25 23 59	232

<sup>a</sup>Observed only at 6 cm.

<sup>b</sup>Observed only at 20 cm.

<sup>c</sup>Contains the phase calibrator, B1748−253.

Table 2. VLBI Sources

Name	6 cm		3.6 cm		1.3 cm	
	$S$ (mJy)	$\theta$ (mas)	$S$ (mJy)	$\theta$ (mas)	$S$ (mJy)	$\theta$ (mas)
1LC 358.439−0.211	< 5.9	>240	< 5.8	>190	< 41	>20
B1739−298 <sup>a</sup>	55.6	27.9	2.5	< 55	< 54	>60
1LC 359.872+0.178	< 5.9	>240	< 3.5	>190	< 32	>58
1LC 0.846+1.173	< 6.9	>390	< 16	>160	< 32	>60
B1741−312 <sup>b</sup>	406	18.2	530	7.2	506	1.3
Sgr A*	420	51.6	510	16.6	860	2.3

<sup>a</sup>Galactic coordinates  $\ell = 358.918$ ,  $b = 0.073$

<sup>b</sup>Galactic coordinates  $\ell = 357.862$ ,  $b = −0.997$